R. & M. No. 2858
(14,474)
A.R.C. Technical Report

MINISTRY OF SUPPLY

AERONAUTICAL RESEARCH COUNCIL
REPORTS AND MEMORANDA

Velocity Distribution on Thin Tapered Wings with Fore-and-aft Symmetry and Spanwise Constant Thickness Ratio at Zero Incidence

By

S. NEUMARK, Techn.Sc.D., A.F.R.Ae.S.,
and
J. COLLINGBOURNE, B.Sc.

LONDON : HER MAJESTY'S STATIONERY OFFICE
1954
PRICE 11*s* 6*d* NET

Velocity Distribution on Thin Tapered Wings with Fore-and-aft Symmetry and Spanwise Constant Thickness Ratio at Zero Incidence

By

S. NEUMARK, Techn.Sc.D., A.F.R.Ae.S., and J. COLLINGBOURNE, B.Sc.

COMMUNICATED BY THE PRINCIPAL DIRECTOR OF SCIENTIFIC RESEARCH (AIR), MINISTRY OF SUPPLY

Reports and Memoranda No. 2858*

June, 1951

Summary.—This report is a continuation of three earlier ones by the present authors[1, 2, 3] (1947–9) and contains a theoretical investigation of subsonic flow past thin tapered unswept wings (of full or cropped-rhombus plan form), at zero incidence. Only the case of spanwise constant thickness ratio is considered in this first attempt although alternative cases also merit attention. The first order method of linear perturbation based on continuous systems of sources and sinks is shown to be still applicable to tapered wings, although mathematical difficulties are greatly increased. These have been overcome, at least in the simple case of the biconvex parabolic profile, so as to give general solutions and computable formulae for the velocity distribution over the entire wing area. Complete detailed solutions for the mid-chord line have been worked out numerically and two examples of complete numerical solutions, with corresponding isobar patterns, for the entire wing area are presented. These results are sufficient to illustrate the effect of uniform taper on the velocity field of unswept wings, and lead to a number of general conclusions. The most important of these is that, although taper brings about noticeable decrease of supervelocities at the centre, higher values are encountered further outboard so that, for cropped plan forms, two symmetrically placed maximum suction areas arise inside the two half-wings. These are relevant for determining critical Mach numbers, and the effect of taper may be, according to choice of geometrical parameters, either beneficial or detrimental as to the values of M_{crit}, but practically never very considerable.

The method will still be applicable to the more general, and more important, case of tapered swept-back wings, especially for delta wings, and a general solution for the velocity distribution in the central sections of such wings is given in Appendix I and shown to be consistent with the earlier solution for untapered swept wings. However, for applying the method successfully (up to detailed numerical investigation) to the more general case, automatic high-speed integrating machinery seems indispensable—to replace classical methods of transforming integrals and manual computing, as used in the past and in the present report.

1. *Introduction.*—In two previous reports by the present authors[1, 2] (1947–9), solutions were given of the velocity distribution on thin untapered swept-back wings of infinite and finite aspect ratio at zero incidence and mainly for the simplest case of the biconvex parabolic profile. The results were extended to other profiles by the present author in Ref. 3 (1949).

The object of the present paper is to continue from this point and to find the velocity distribution on thin tapered wings with zero sweep-back of the mid-chord line. The method used to solve this problem is again that of linear perturbation in which the wing is replaced by

* R.A.E. Report Aero. 2432, received 13th December, 1951.

a system of sources and sinks; the required velocity field is then approximately obtained as that of the velocity components, in the plane of the chord lines, given by this source system. The distribution of sources and sinks is chosen so that the v_z component is obtained correct to the first order of thickness ratio.

The supervelocity v_x may then be determined by direct integration. The v_y component has not been calculated for the case of tapered wings as it was felt that the work entailed would not be justified; v_y contributes only second order corrections to the resultant supervelocity, and the general trend can be implied from the previous work.

The tapered plan forms considered in this paper (Figs. 2 and 3) must be defined by a carefully chosen set of geometrical parameters. We introduce first an important new parameter ε, the spanwise rate of decrease of the semi-chord, which has been termed ' coefficient of convergence '. This seems to be the most rational measure of taper, and becomes zero for untapered wings; it is the only parameter needed to determine the shape of a full rhombus plan form. A cropped straight tapered wing is then obtained by cutting off certain triangular portions at the tips, and to determine these, another parameter ψ—the ratio of tip chord to root chord (the usual ' taper ratio ') has been used. If, finally, a swept-back tapered wing is to be considered, a third parameter φ_0, angle of sweep of the mid-chord line, is introduced. This set of parameters must not be considered as standard but it has been found the most convenient for the analytical solution of zero-lift problems. Some alternative sets of parameters for swept-back wings have been proposed by Thomas[4] (1951), and Warren[5] (1951), which may be more suitable for other purposes.

As in Ref. 2, it was decided that to minimise the possibility of errors we should begin with the simpler cases and build up to the more complex. Both algebraic and numerical checks are then available at each stage of the calculations. Furthermore, in order to reduce the complications throughout, it has been decided to consider only the case of a wing with a biconvex parabolic profile along the entire span. This does not mean, however, that the method cannot be extended to cover other profiles although the formulae would then become more complicated. To have the wing surface completely defined, we must then still determine the spanwise variation of the profile thickness ratio ϑ. It has been decided to limit this investigation to the case of ϑ constant throughout the span; this is geometrically the simplest assumption but, curiously enough, not that leading to the simplest mathematics (this would be simpler, *e.g.*, for wings with constant thickness spanwise, *i.e.*, with thickness ratio increasing towards the tips in inverse proportion to the chords; or, *vice versa,* for wings with thickness ratio decreasing proportionally to the chords, *i.e.*, with thickness decreasing as chord squared). However, our assumption seems to be the most appropriate for the first theoretical attempt, and it is the only one which gives a reasonable wing in the case of the full-rhombus plan form*.

The formulae for the supervelocity at the central section and, more particularly, for the central point of this section, for both full and cropped-rhombus wings, have been found first of all; and suitable computational methods have been evolved followed by a fairly extensive numerical investigation.†

Similar but more complicated results were worked out subsequently for the velocity distribution over the mid-chord lines of both full and cropped-rhombus wings, and finally for the complete velocity distribution over the entire wing surface of both wings.

As work proceeded from the particular to more general solutions, the complexity of formulae and computational methods increased rapidly. The integrals involved, unlike those in the previous investigations, are no longer expressible in terms of elementary or tabulated functions and have to be expanded into infinite series before they can be evaluated. Special procedures

* The case of a tapered swept-back wing with thickness ratio proportional to the chord was treated briefly by A. Fiul[8] (1948), obviously because of the simpler mathematical analysis, but only very few numerical examples were presented. The case merits a fuller investigation.

† Preliminary results for this case were found by the present author already in 1948 and presented in Ref. 6.

are needed to ensure sufficiently rapid convergence of these series. It has, therefore, proved impossible to work out more than a few typical numerical examples for the more general cases; especially for the velocity distribution over the entire wing area, including isobar patterns. There seems to be no need for extensive calculations of this sort, as the few examples presented appear to be sufficient for obtaining a clear picture of the velocity fields and general trends.

The main *conclusions* from this investigation may be summarized as follows:

(*a*) The method has been proved applicable to the case of straight tapered wings but the difficulties of computation are serious. It has been possible to overcome these, at least in the few examples which have been worked out and which suffice to give a general picture of the effect of taper.

(*b*) The examination of the effect of taper at the *central section* of a straight tapered wing, especially at the centre, is comparatively easy, and has been made in a fairly exhaustive manner so that a wide range of parameters ε and ψ has been covered. The local maximum supervelocity occurs at the centre (for the biconvex parabolic profile) and the graphs on Figs. 4 and 5 give a comprehensive picture. It appears that, for a full rhombus wing, with increasing ε, this maximum decreases markedly, and by cropping the wing (*i.e.*, increasing ψ from zero upwards), we achieve a further decrease in maximum at the centre.

(*c*) The latter conclusion might lead to the belief that tapering a wing should be fundamentally beneficial so as to raise the critical Mach number. However, the case is not nearly as simple as that. The examination of velocity distribution along the *mid-chord line* (the locus of maxima at all spanwise stations) shows, rather surprisingly, that the supervelocity has a clear tendency to increase when moving outboard from the centre (Figs. 6, 10 and 11). In the case of a full rhombus (Fig. 6) this tendency develops unchecked right to the sharp tips where our theory gives a logarithmically infinite value; but already, at little more than half-way along the semi-span, the maximum supervelocity reaches the two-dimensional value. Therefore, if only small bits are cut off at the tips of a rhombus wing, such a wing would present no advantage over an untapered one, and might even be at a disadvantage. The interesting difference is that now the danger sections would be located near the tips rather than at the centre.

(*d*) When cropping a rhombus wing by a considerable amount, *i.e.*, introducing larger values of the parameter ψ, we encounter again, as for untapered wings, a decrease in the maximum supervelocity at the tips (Figs. 10 and 11) to roughly half the values at the same spanwise stations for the uncropped wing. This tip effect of reducing the supervelocity begins to check more and more the tendency for it to increase along the entire span, even quite near to the central section, when both ε and ψ are large. A cropped tapered wing, therefore, may have somewhat better characteristics, as far as critical Mach number is concerned, than an untapered wing (Fig. 12). The danger section is more often than not at some spanwise station different from the central one.

(*e*) It has been found possible, finally, to work out the velocity distribution over the entire wing area, in order to obtain isobar patterns; two examples of such patterns are given in Figs. 13 and 14 (and discussed in more detail elsewhere in this report). It would probably have been very difficult to guess at even the most approximate pictures of the isobars disposition without this long and difficult computation, and the effort seems to be justified for the diagrams are so much different from what was obtained previously for untapered wings. The isobar patterns will, of course, vary with geometrical parameters of the plan form, and they will be considerably affected by modifying the wing profile. General trends due to taper seem to be clearly demonstrated, however.

(*f*) The results presented may be used for calculating critical Mach numbers for straight tapered wings, but this has not been attempted here. A short qualitative discussion shows that critical Mach numbers may be reasonably defined only for cropped wings; that the first danger

points will usually be located symmetrically at spanwise stations within both half-wings (practically never at the centre if the profile has fore-and-aft symmetry); and, finally, that the advantage likely to be gained by taper will not be considerable for unswept wings (Fig. 12).

(*g*) We may expect the theory still to be applicable to the most general case (swept tapered wings, in particular delta wings), and partial results (for the central section) are presented in Appendix I of this report. These are shown to be consistent with the previous ones for swept untapered wings, but no attempt at computation has been made thus far. It is clear that, in this paper, we have reached the point beyond which the general integrals of the theory can no longer be evaluated by a combination of analysis and manual computation without prohibitive labour. The most important case, practically, of sweepback with taper (including the delta wing) is still more difficult, particularly as it necessitates exploration of the entire wing in almost every case. It is therefore proposed to solve this final problem with the aid of automatic integrators.

Acknowledgements are due to R. P. Purkiss who did an earlier part of the computational work, and to Miss S. A. Brown and W. P. Gillott who completed the remaining greater part of this and prepared the illustrations.

2. *Preliminary Considerations.*—A wing of arbitrary plan form and with any symmetrical profile is shown in Fig. 1. P is any point on the surface of this wing and has co-ordinates (x, y). If we replace the wing by a continuous system of sources and sinks, and if Q represents a source element of area $(d\bar{x}\ d\bar{y})$, then the induced velocity in the x-direction at P due to the source element at Q is:

$$v_x = \iint_S \frac{q\ d\bar{x}\ d\bar{y} \cos\beta}{4\pi l^2}, \qquad (2.1)$$

where q is the source strength at Q (per unit area), l denotes the distance QP, β is the angle QP makes with the x-axis, and the integration must be performed over the entire wing area S.

If the equation of the wing surface is:

$$z = F(x,y), \qquad (2.2)$$

then

$$q = -2U \cdot F_x'(\bar{x},\bar{y}), \qquad (2.3)$$

and hence, from (2.1):

$$-\frac{2\pi v_x}{U} = \iint_S \frac{F_x'(\bar{x},\bar{y})(x-\bar{x})\ d\bar{x}\ d\bar{y}}{[(x-\bar{x})^2+(y-\bar{y})^2]^{3/2}}. \qquad (2.4)$$

In this report only v_x has been considered as v_y contributes only second-order corrections to the supervelocity and has little practical importance.

A less general wing planform is shown in Fig. 2 with straight leading and trailing edges. For describing this wing we use three geometric parameters: the taper ratio $\psi = c_t/c_r$, the angle of sweepback of the mid-chord line φ_0, and the coefficient of convergence $\varepsilon = b/s'$, which is the rate of decrease of the semi-chord with the spanwise co-ordinate* (*see* Fig. 2).

* The parameters for such a wing more usual in practical engineering would be: taper ratio ψ, aspect ratio A, and the angle of sweepback of some representative line, *e.g.*, the leading edge or the quarter-chord line. For the present calculations, however, the parameters defined in the text were found more convenient. The following formulae connect different parameters:

$$\left\{\begin{aligned} A &= \frac{2}{\varepsilon}\frac{1-\psi}{1+\psi}, \\ \tan\varphi_L &= \tan\varphi_0 + \varepsilon, \\ \tan\varphi_{1/4} &= \tan\varphi_0 + \tfrac{1}{2}\varepsilon. \end{aligned}\right.$$

Several alternative sets of parameters are suggested and discussed by Thomas[4] (1951) and Warren[5] (1951).

The plan form of this wing has a discontinuity at the central section and it is, therefore, necessary to consider the supervelocity as composed of two parts, namely the contributions to it of the right-hand half of the wing (v_{xr}), and the left-hand half (v_{xl}). The former becomes:

$$-\frac{2\pi v_{xr}}{U} = \int_0^s d\bar{y} \int_{\bar{x}_T}^{\bar{x}_L} \frac{(x-\bar{x})F_x'(\bar{x},\bar{y})}{[(x-\bar{x})^2+(y-\bar{y})^2]^{3/2}}\, d\bar{x}\,, \quad \ldots \quad \ldots \quad \ldots \quad \ldots \quad (2.5)$$

where $\bar{x}_L$, $\bar{x}_T$ are the values of $\bar{x}$ at the leading and trailing edges respectively and defined by the formulae:

$$\left.\begin{aligned} \bar{x}_L &= b - \bar{y}(\tan\varphi_0 + \varepsilon) = b - \bar{y}\tan\varphi_L\,, \\ \bar{x}_T &= -b - \bar{y}(\tan\varphi_0 - \varepsilon) = -b - \bar{y}\tan\varphi_T\,. \end{aligned}\right\} \quad \ldots \quad \ldots \quad (2.6)$$

There will be an analogous formula for v_{xl} which will differ only from (2.5) by the sign of y; for the contributions of the left-hand half-wing at a point P on the right-hand half-wing will be exactly the same as those induced by the right-hand half-wing at a symmetrically placed point P_1 on the left-hand half-wing (*see* Fig. 3).

Integrating (2.5) by parts with respect to $\bar{x}$ we obtain:

$$-\frac{2\pi v_{xr}}{U} = \int_0^s \left[\left| \frac{F_x'(\bar{x},\bar{y})}{[(x-\bar{x})^2+(y-\bar{y})^2]^{1/2}} \right|_{\bar{x}_T}^{\bar{x}_L} - \int_{\bar{x}_T}^{\bar{x}_L} \frac{F_x''(\bar{x},\bar{y})}{[(x-\bar{x})^2+(y-\bar{y})^2]^{1/2}}\, d\bar{x} \right] d\bar{y}\,. \quad (2.7)$$

It will be seen that the first term of (2.7) can always be integrated in terms of algebraic functions or elementary transcendents if $F(x,y)$ is a polynomial. The second term, however, is more complex; for, if $F(x,y)$ is a polynomial, the first integration with respect to $\bar{x}$ will give the integrand for the second integral in terms of algebraic functions and elementary transcendents and the subsequent integration (with respect to $\bar{y}$) will therefore be complex and will generally lead to higher transcendents. In view of the increased computational work involved in evaluating such integrals, it has been decided that we should consider first only a simple case of a wing with biconvex parabolic profile, the equation of whose surface (right-hand half) is:

$$F(x,y) = \vartheta b\left(1 - \frac{y}{s'}\right)\left(1 - \frac{(x + y\tan\varphi_0)^2}{b^2(1-y/s')^2}\right), \ldots \quad \ldots \quad \ldots \quad \ldots \quad \ldots \quad (2.8)$$

where $b(1-y/s') > x + y\tan\varphi_0 > -b(1-y/s')$, $0 < y < s$.

The second derivative of (2.8) with respect to x is independent of x. It may be mentioned that the thickness ratio ϑ in (2.8) may still be chosen arbitrarily as either constant or as any function of the local chord, *i.e.*, of $(1-y/s')$. In this report, only a wing with zero angle of sweepback of the mid-chord line ($\varphi_0 = 0$) and with ϑ constant along the entire span has been considered. Two cases have been investigated, namely, the rhombus wing with zero taper ratio ψ, and the cropped-rhombus wing with arbitrary taper ratio.

It should be noticed that the method of evaluating supervelocities for tapered wings used here differs from that used in the previous reports[1, 2] in that the integration has been performed chordwise first and spanwise later, whereas in Refs. 1 and 2 the spanwise integration was performed first. This order of integration was found to be more convenient in this case. An interesting fact is that if the velocity distribution at the central section of a swept-back fully tapered wing is found by this method directly (by putting $y = 0$ before integration) then in the limiting case $\varepsilon \to 0$ (*i.e.*, the wing becomes an infinite swept-back one) the correct expression for supervelocity, as known from Ref. 1, is obtained. Appendix I shows this in more detail. This seems to indicate that integrating chordwise before spanwise is to be preferred, as the same results do not follow if the order of integration is reversed while still putting $y = 0$ before integrating (*see* Ref. 1, sections 4, 5 and 6).

3. *Velocity Distribution over Rhombus Wing with Biconvex Parabolic Profile and Spanwise Constant Thickness Ratio.*—The rhombus wing plan form to be considered is shown in Fig. 3, and it will be seen that $s = s'$, $\psi = 0$, $\varphi_0 = 0$, $\tan \varphi_L = \varepsilon$ and $\tan \varphi_T = -\varepsilon$. The equation of the surface (right-hand half) becomes, from (2.8):

$$z = F(x,y) = \vartheta b\left(1 - \frac{y}{s'}\right)\left(1 - \frac{x^2}{b^2(1 - y/s')^2}\right), \qquad (3.1)$$

where $b(1 - y/s') > x > -b(1 - y/s')$, $\quad 0 < y < s'$,

and
$$F_x'(x,y) = -\frac{2\vartheta x}{b(1 - y/s')}, \qquad (3.2)$$

$$F_x''(x,y) = -\frac{2\vartheta}{b(1 - y/s')}. \qquad (3.3)$$

The thickness ratio ϑ in the above equations may still be chosen arbitrarily but if we now assume ϑ to be constant along the span and then substitute (3.2), (3.3) in (2.7), we obtain, after integrating with respect to $\bar{x}$, the supervelocity induced by the right-hand half of the wing surface at P:

$$\frac{\pi v_{xr}}{U\vartheta} = \int_0^{s'} \frac{d\bar{y}}{r_1} + \int_0^{s'} \frac{d\bar{y}}{r_2} + \int_0^{s'} \frac{1}{b(1 - \bar{y}/s')} \ln\left\{\frac{x - \bar{x}_L + r_2}{x - \bar{x}_T + r_1}\right\} d\bar{y}, \qquad (3.4)$$

where (from 2.6)

and
$$\left.\begin{aligned} \bar{x}_T &= -b + \bar{y}\varepsilon, \\ \bar{x}_L &= b - \bar{y}\varepsilon, \\ r_1^2 &= (x - \bar{x}_T)^2 + (y - \bar{y})^2, \\ r_2^2 &= (x - \bar{x}_L)^2 + (y - \bar{y})^2. \end{aligned}\right\} \qquad (3.5)$$

The supervelocity may be expressed in non-dimensional form by substituting the following in (3.4)*:

$$\left.\begin{aligned} y &= s'\eta', \\ \bar{y} &= s'\bar{\eta}, \\ x &= b(1 - y/s')\xi. \end{aligned}\right\} \qquad (3.6)$$

Then

$$\frac{\pi v_{xr}}{U\vartheta} = \int_0^1 \frac{d\bar{\eta}}{\varrho_1} + \int_0^1 \frac{d\bar{\eta}}{\varrho_2} + \frac{1}{\varepsilon}\int_0^1 \frac{1}{1 - \bar{\eta}} \ln\left(\frac{\varepsilon\xi(1 - \eta') - \varepsilon(1 - \bar{\eta}) + \varrho_2}{\varepsilon\xi(1 - \eta') + \varepsilon(1 - \bar{\eta}) + \varrho_1}\right) d\bar{\eta}, \qquad (3.7)$$

where

$$\left.\begin{aligned} \varrho_1^2 &= (\bar{\eta} - \eta')^2 + \varepsilon^2[\xi(1 - \eta') + 1 - \bar{\eta}]^2, \\ \varrho_2^2 &= (\bar{\eta} - \eta')^2 + \varepsilon^2[\xi(1 - \eta') - (1 - \bar{\eta})]^2. \end{aligned}\right\} \qquad (3.8)$$

The contribution of the left-hand half of the wing to the induced velocity at P may be found in a similar way from (2.4) but it may be more easily obtained directly from (3.7). For, the induced velocity at P due to the left-hand half of the wing is exactly the same as that at P_1

* η' was chosen as the non-dimensional spanwise co-ordinate (varying from 0 to 1 for a full rhombus, and 0 to $(1 - \psi)$ for a cropped wing). This is different from that used in previous reports where the co-ordinate $\eta = y/b$ was taken. ξ is the chordwise non-dimensional co-ordinate and varies from (-1) at the trailing edge to $(+1)$ at the leading edge.

(a point placed symmetrically to P with respect to the central section, in the left-hand half of the wing (*see* Fig. 3)) due to the right-hand half of the wing. This latter supervelocity may be found from (3.4) simply by reversing the sign of y. If we write (3.4) in a shorthand form as

$$\pi v_{x\,r}/U\vartheta = f(x,y)\,, \quad .. \quad .. \quad .. \quad .. \quad .. \quad .. \quad .. \quad .. \quad .. \quad (3.9)$$

then $$\pi v_{x\,l}/U\vartheta = f(x,-y)\,. \quad .. \quad .. \quad .. \quad .. \quad .. \quad .. \quad .. \quad .. \quad (3.10)$$

Non-dimensionally:

$$\frac{\pi v_{x\,r}}{U\vartheta} = g(\xi,\eta') = g\left(\frac{x}{b(1-y/s')}\,,\, y/s'\right), \quad .. \quad .. \quad .. \quad .. \quad .. \quad (3.11)$$

and $$\frac{\pi v_{x\,l}}{U\vartheta} = g\left(\frac{x}{b(1+y/s')}\,,\, -y/s'\right); \quad .. \quad .. \quad .. \quad .. \quad .. \quad .. \quad (3.12)$$

but as ξ is still defined by (3.6) for any point of the right-hand half of the wing, so the contribution of the left-hand half of the wing to the supervelocity at P is:

$$\frac{\pi v_{x\,l}}{U\vartheta} = g\left(\xi\,\frac{1-\eta'}{1+\eta'}\,,\, -\eta'\right). \quad .. \quad .. \quad .. \quad .. \quad .. \quad .. \quad (3.13)$$

In other words, the contribution of the left-hand half is given directly from (3.7) by reversing the sign of η' and replacing ξ by $\xi\,\dfrac{1-\eta'}{1+\eta'}$. This method of conversion must be used with caution throughout further calculations, however, as it is not applicable at every stage (*see* Appendix II).

The contribution of the left-hand half of the wing is therefore:

$$\frac{\pi v_{x\,l}}{U\vartheta} = \int_0^1 \frac{d\bar{\eta}}{\varrho_3} + \int_0^1 \frac{d\bar{\eta}}{\varrho_4} + \frac{1}{\varepsilon}\int_0^1 \frac{1}{1-\bar{\eta}} \ln\left(\frac{\varepsilon\xi(1-\eta') - \varepsilon(1-\bar{\eta}) + \varrho_4}{\varepsilon\xi(1-\eta') + \varepsilon(1-\bar{\eta}) + \varrho_3}\right) d\bar{\eta}\,, \quad (3.14)$$

where
$$\left.\begin{aligned} \varrho_3^{\,2} &= (\bar{\eta}+\eta')^2 + \varepsilon^2[\xi(1-\eta') + 1 - \bar{\eta}]^2\,, \\ \varrho_4^{\,2} &= (\bar{\eta}+\eta')^2 + \varepsilon^2[\xi(1-\eta') - (1-\bar{\eta})]^2\,. \end{aligned}\right\} \quad .. \quad .. \quad .. \quad .. \quad (3.15)$$

The complete supervelocity at P is thus the sum of (3.7) and (3.14). To evaluate these formulae the terms involving logarithms were integrated by parts, and the velocity distribution can then be reduced to the following form:

$$\left.\begin{aligned} -\pi v_{x\,r}/U\vartheta &= I_1 + I_2\,, \\ -\pi v_{x\,l}/U\vartheta &= I_3 + I_4\,, \end{aligned}\right\} \quad .. \quad .. \quad .. \quad .. \quad .. \quad .. \quad .. \quad .. \quad (3.16)$$

with
$$\left.\begin{aligned} I_1 &= -\int_0^1 \left\{1 + (1-\eta')(1+\xi)\,\frac{\ln(1-\bar{\eta})}{\bar{\eta}-\eta'}\right\}\frac{d\bar{\eta}}{\varrho_1}\,, \\ I_2 &= -\int_0^1 \left\{1 + (1-\eta')(1-\xi)\,\frac{\ln(1-\bar{\eta})}{\bar{\eta}-\eta'}\right\}\frac{d\bar{\eta}}{\varrho_2}\,, \\ I_3 &= -\int_0^1 \left\{1 + (1+\eta')\left(1+\xi\,\frac{1-\eta'}{1+\eta'}\right)\frac{\ln(1-\bar{\eta})}{\bar{\eta}+\eta'}\right\}\frac{d\bar{\eta}}{\varrho_3}\,, \end{aligned}\right\} \quad .. \quad .. \quad (3.17)$$

and
$$I_4 = -\int_0^1 \left\{1 + (1+\eta')\left(1-\xi\,\frac{1-\eta'}{1+\eta'}\right)\frac{\ln(1-\bar{\eta})}{\bar{\eta}+\eta'}\right\}\frac{d\bar{\eta}}{\varrho_4}\,.$$

Now, if η' is zero, we obtain from (3.11) the *supervelocity distribution at the central section of a rhombus wing*. For this particular section, of course, the contributions of the two halves of the wing are equal. The total supervelocity at the central section is then:

$$-\pi v_x/2U\vartheta = I_1 + I_2, \qquad (3.18)$$

where

$$\left.\begin{aligned} I_1 &= -\int_0^1 \left\{ 1 + (1+\xi)\frac{\ln(1-\bar{\eta})}{\bar{\eta}} \right\} \frac{d\bar{\eta}}{\{\bar{\eta}^2 + \varepsilon^2(\xi + 1 - \bar{\eta})^2\}^{1/2}} \\ I_2 &= -\int_0^1 \left\{ 1 + (1-\xi)\frac{\ln(1-\bar{\eta})}{\bar{\eta}} \right\} \frac{d\bar{\eta}}{\{\bar{y}^2 + \varepsilon^2(\xi - 1 + \bar{\eta})^2\}^{1/2}}. \end{aligned}\right\} \qquad (3.19)$$

If, in addition, ξ is equal to zero, we have the value of the *supervelocity at the mid-point of the central section :*

$$-\frac{\pi v_x}{4U\vartheta} = -\int_0^1 \left\{ 1 + \frac{\ln(1-\bar{\eta})}{\bar{\eta}} \right\} \frac{d\bar{\eta}}{\{\bar{\eta}^2 + \varepsilon^2(1-\bar{\eta})^2\}^{1/2}} \qquad (3.20)$$

Next let us put $\xi = 0$ in (3.16) and (3.17) and we then obtain the *supervelocity distribution along the mid-chord line* (y-axis in Fig. 3). This is then given by:

$$-\frac{\pi v_x}{2U\vartheta} = -\int_0^1 \left\{ 1 + (1-\eta')\frac{\ln(1-\bar{\eta})}{\bar{\eta} - \eta'} \right\} \frac{d\bar{\eta}}{\varrho_1} - \int_0^1 \left\{ 1 + (1+\eta')\frac{\ln(1-\bar{\eta})}{\bar{\eta} + \eta'} \right\} \frac{d\bar{\eta}}{\varrho_3}, \qquad (3.21)$$

the expressions for ϱ_1, ϱ_2, ϱ_3, ϱ_4 being now:

$$\left.\begin{aligned} \varrho_1^2 = \varrho_2^2 &= (\bar{\eta} - \eta')^2 + \varepsilon^2(1-\bar{\eta})^2, \\ \varrho_3^2 = \varrho_4^2 &= (\bar{\eta} + \eta')^2 + \varepsilon^2(1-\bar{\eta})^2. \end{aligned}\right\} \qquad (3.22)$$

It may be seen that the first integral (which represents the right-hand half contribution) has an infinite value for $\eta' = 1$.

The integrals involved could not be evaluated exactly in terms of elementary or tabulated functions, and it has been decided to perform the integration by expanding the integrands into convergent power series and hence finding a sufficient number of terms in each series to ensure a reasonable degree of accuracy. Details of the expansion of these integrals are given in Appendix II. The necessity of having to calculate the integrals by summing a number of terms of infinite series naturally entailed a great deal of computation. Velocity distribution over the entire wing and the isobar pattern has, therefore, been found for only one example of a rhombus wing with a coefficient of convergence $\varepsilon = 0{\cdot}3$.

In view of the computational difficulties the first calculations were made for the simplest case of the wing centre only. Values of this induced velocity were found for a range of ε from 0 to 1·5. The values of the supervelocity ratio $-\pi v_x/4U\vartheta$ have been plotted against ε for the central point of the central section of a rhombus wing and these values are given in Table 1 (figures corresponding to $\psi = 0$ for various ε); the graph of this variation is shown in Fig. 4 ($\psi = 0$ curve). It would appear from these results that tapering the unswept wing has a wholly beneficial effect, but this cannot be accepted until a more detailed investigation has been made.

The next step in the calculations is to find the supervelocity at various spanwise positions along the *mid-chord line* ($\xi = 0$) which, by comparison with the results for untapered unswept wings with biconvex parabolic profile, will probably be the locus of the local maxima. This spanwise supervelocity distribution has been found for rhombus wings with ε varying from 0 to 1·0. These results are given in Table 2 and Fig. 6. It is clear from these that the optimistic picture of the effect of taper on an unswept wing given by Fig. 4 is partly an illusion for, although v_x at the central point decreases as ε increases, Fig. 6 shows that v_x increases along the span and finally tends to a logarithmic infinity as the tip is approached.

The singularity at the sharp wing tip, consisting of a logarithmically infinite supervelocity when approaching the tip along the mid-chord line, may seem surprising*. The singularity at the right-hand tip is due to the source-sink system of the right-hand half-wing only because, obviously, the other half-wing contributes merely a small finite increase. Fig. 7 represents, as an example, the respective contributions of the right-hand half-wing (curve A) and the left-hand half-wing (curve B) to the supervelocity along the right-hand half of the mid-chord line, in the case $\varepsilon = 0{\cdot}3$; the total being shown by curve C which corresponds to the $0{\cdot}3$ curve of Fig. 6. The curve A represents the mid-chord line distribution for a separate *triangular wing* (half of the full rhombus) and exhibits the same sort of singularity at the tip as previously observed on curve C. Suppose now that the triangular planform gradually expands leftwards from its fixed tip, the coefficient ε being kept constant so that the shape of the triangle remains unchanged, its scale only being increased. Then curve A still represents the mid-chord supervelocity distribution if it is kept in mind that η' is a non-dimensional quantity denoting the fraction of the (gradually growing) span. If, however, a point on the mid-chord line, at a fixed distance from the fixed tip, is considered, then η' assumes higher and higher values as the wing expands leftwards, and the supervelocity increases accordingly. When the span ultimately becomes infinite, η' at all points at a finite distance from the tip approaches 1, and supervelocities rise to infinity. This can also be checked immediately by examining the corresponding formula (first integral in 3.21) with $-\infty$ as the lower limit of integration. It would be vain, therefore, to try to introduce the concept of a 'semi-infinite triangular plan form' as a simple representative of tapered wings†, analogous to semi-infinite or infinite untapered wings, which served us so well previously.

It would have been difficult to predict whether the supervelocities on a fully tapered (in particular triangular) wing should be generally greater or less than those on an untapered (especially two-dimensional) one. At any section, the contribution of the adjacent tapering part must be smaller, that of the adjacent diverging part greater, than the corresponding amounts in the case of a constant-chord wing, but it is not clear beforehand which effect will prevail. Our analysis shows that the increasing tendency has the upper hand if the wider part occupies a sufficiently large proportion of the span, more and more so as the section approaches the sharp tip.

It will be seen, therefore, that taper may have a detrimental effect on the critical Mach number, especially if the wing has fairly sharp tips. This, however, is not so serious as it appears at first, for the taper ratio $\psi = c_t/c_r$ will always be an appreciable fraction, as sharp tips never occur in actual design. The supervelocities on wings with $\psi \neq 0$ are investigated in the next section.

Before leaving the rhombus wing, it was thought that an attempt should be made to determine the velocity field over the entire surface of such a wing. The amount of computation involved made it impossible to consider more than one case, and a wing with $\varepsilon = 0{\cdot}3$ has been chosen. The supervelocities were found at various spanwise positions, and the isobars over the entire wing were found from these curves. Fig. 8 and Table 3 show the variation of $-\pi v_x/4U\vartheta$ with ξ and η' for this wing, and Fig. 13 is a diagram of the isobars. It will be seen that the results confirm the fact that the sectional maximum supervelocities occur along the mid-chord line for the biconvex parabolic profile and that, therefore, Fig. 6 does indeed give the variation of the local maxima spanwise with coefficient of convergence ε.

---

* It may be stressed that this singularity has been obtained entirely on the basis of the first-order method, and the results of an exact theory (or, at least, of a higher order approximation) may be different. No appreciable corrections should be expected within a major part of the span, but the nature of singularities at the sharp tips is unpredictable for the time being, so that it must be left as an open question whether the supervelocity along the mid-chord line really increases indefinitely towards the tips in the exact solution. The answer may be different according to whether we consider a flow past a given wing (the system of sources and sinks being then slightly modified), or a flow with the assumed system of sources and sinks (in which case the wing shape would be somewhat altered). The problem is certainly an extremely difficult one, but its interest is purely academic, as only minute tip portions are involved. It will be seen in section 4 that this type of singularity will not occur at the tips of cropped wings, the only ones likely to be used in design.

† At least on the assumption of thickness ratio being invariable spanwise, but alternative assumptions do not seem promising for any practical purpose.

The isobar pattern in Fig. 13 is very instructive, especially if compared to that for an untapered finite wing (*see, e.g.*, Fig. 26 of Ref. 2) from which it differs in a striking way. The dominating feature is that all isobars converge to the sharp tip corner which presents a peculiar singularity. It is obvious that all isobars corresponding to low and all negative supervelocities must converge to this corner, as the wing profile near to it contracts to zero length, and thus the stagnation points and points with gradually increasing velocities all tend to coalesce. However, isobars with indefinitely increasing positive supervelocities also radiate from this same point, although their dimensions become decreasingly small. This could be expected because the supervelocity along the mid-chord line has been shown to tend to logarithmic infinity at this point. The mathematical singularity is physically of little importance by itself, but it results in the isobars with high numbers (high-suction lines) doubling back on themselves and becoming closed contours within one of the half-wings, close to the mid-chord line; they do not reach the central section where the local maximum (0·897 in the case of Fig. 8) is lower than their own parameter. Naturally, lower isobars do reach the central section which they cross at right-angles, and thus run through the entire wing span. There obviously exists one isobar (corresponding to the central section maximum) which separates the two groups, and this consists of two branches with a double point at the origin O. The entire picture thus differs from that of an untapered wing (Ref. 2, Fig. 26) in that the higher isobars are concave to the tip instead of to the central section*.

Fig. 13 represents, of course, only one particular case (for $\varepsilon = 0{\cdot}3$) but this example is typical, as may be concluded from the diagram in Fig. 6, which shows that the maximum local supervelocities always increase continuously from centre to tip, the slope increasing with ε. The isobar patterns for various ε will, therefore, always resemble that of Fig. 8, the only effect of increasing ε being that the higher (closed) isobars will be more crowded spanwise. A rough sketch for arbitrary ε may be drawn by using a corresponding curve from Fig. 6 using in addition, if possible, the velocity distributions in the central section.

Finally, if another profile, differing from the biconvex parabolic (in particular, not symmetrical fore-and-aft) is chosen, the isobar pattern will be essentially similar to that of Fig. 13, but there will be no symmetry about the y-axis, the maximum supervelocities of particular sections will be numerically changed (generally increased) and be on a curvilinear locus, and the isobars will be more crowded in the region of greater curvature of the profile, etc. Apart from such distortion, we should not expect any qualitative changes, especially for moderate ε, unless the profile itself is a bad shape with irregular two-dimensional characteristics.

As regards critical Mach numbers, the position is rather peculiar, owing to the theoretically infinite supervelocity at the sharp tip which seems to be the first danger point. It is impossible to calculate the lower critical, and its significance would anyhow be negligible because the area initially affected would be small. However, it is clear that, at increasing speeds, shock-waves would first appear in tip areas to spread gradually inwards until they reach the central section. The matter does not merit a numerical examination as sharp-tipped wings are never used in design.

4. *Velocity Distribution over a Cropped-Rhombus Wing with Biconvex Parabolic Profile and Spanwise Constant Thickness Ratio.*—The cropped-rhombus wing plan form which has been considered is shown in Fig. 3, and in this case $s = s'(1 - \psi)$, where $0 < \psi < 1$.

As the velocity distribution has already been calculated for the rhombus wing it is convenient to calculate the effect of the ' cut off ' tip triangles and subtract this from that of the complete rhombus wing. In this way the additional computation is shortened because the terms of the new series are small and so only a few of them need to be calculated to obtain the required accuracy. Also, the effect of the tip triangles on sections near the centre, to be subtracted from the full-rhombus values, is often so small as to be negligible.

* This isobar pattern is obtained, of course, on the basis of the first-order theory. An exact pattern will only deviate slightly within a major part of the planform, but some alterations, difficult to predict, may occur in the nearest neighbourhood of the sharp tips.

The velocity contribution of the ' cut off ' right-hand tip triangle is given by (3.7) and (3.8) when a suitable change of the limits of integration is made; thus:

$$\frac{\pi\hat{v}_{xr}}{U\vartheta} = \int_{1-\psi}^{1} \frac{d\bar{\eta}}{\varrho_1} + \int_{1-\psi}^{1} \frac{d\bar{\eta}}{\varrho_2} + \frac{1}{\varepsilon}\int_{1-\psi}^{1} \frac{1}{1-\bar{\eta}_r} \ln\left\{\frac{\varepsilon\xi(1-\eta') - \varepsilon(1-\bar{\eta}) + \varrho_2}{\varepsilon\xi(1-\eta') + \varepsilon(1-\bar{\eta}) + \varrho_1}\right\} d\bar{\eta}\,, \qquad (4.1)$$

where ϱ_1 and ϱ_2 are defined in (3.8), and the non-dimensional co-ordinates η', $\bar{\eta}$ and ξ are the same as before (*see* 3.6).

As for the rhombus wing, the contribution of the left-hand tip triangle is obtained by replacing η' by $(-\eta')$ and ξ by $\left(\xi\,\frac{1-\eta'}{1+\eta'}\right)$ in (4.1).

The logarithmic term is then integrated by parts, and the limits substituted where possible; the formula (4.1) then reduces to:

$$\left.\begin{aligned} -\pi\hat{v}_{xr}/U\vartheta &= \Omega + \bar{I}_1 + \bar{I}_2\,, \\ -\pi\hat{v}_{xl}/U\vartheta &= \Lambda + \bar{I}_3 + \bar{I}_4\,, \end{aligned}\right\} \qquad (4.2)$$

where

$$\left.\begin{aligned} \Omega &= \frac{1}{\varepsilon}\ln\psi\ln\left[\frac{\varepsilon\xi(1-\eta') + \varepsilon\psi + \hat{\sigma}_{1,1-\psi}}{\varepsilon\xi(1-\eta') - \varepsilon\psi + \hat{\sigma}_{2,1-\psi}}\right], \\ \Lambda &= \frac{1}{\varepsilon}\ln\psi\ln\left[\frac{\varepsilon\xi(1-\eta') + \varepsilon\psi + \hat{\sigma}_{3,1-\psi}}{\varepsilon\xi(1-\eta') - \varepsilon\psi + \hat{\sigma}_{4,1-\psi}}\right], \\ \bar{I}_1 &= -\int_{1-\psi}^{1}\left[1 + (1-\eta')(1+\xi)\frac{\ln(1-\bar{\eta})}{\bar{\eta}-\eta'}\right]\frac{d\bar{\eta}}{\varrho_1}\,, \\ \bar{I}_2 &= -\int_{1-\psi}^{1}\left[1 + (1-\eta')(1-\xi)\frac{\ln(1-\bar{\eta})}{\bar{\eta}-\eta'}\right]\frac{d\bar{\eta}}{\varrho_2}\,, \\ \bar{I}_3 &= -\int_{1-\psi}^{1}\left[1 + (1+\eta')\left(1+\xi\frac{1-\eta'}{1+\eta'}\right)\frac{\ln(1-\bar{\eta})}{\bar{\eta}+\eta'}\right]\frac{d\bar{\eta}}{\varrho_3}\,, \\ \bar{I}_4 &= -\int_{1-\psi}^{1}\left[1 + (1+\eta')\left(1-\xi\frac{1-\eta'}{1+\eta'}\right)\frac{\ln(1-\bar{\eta})}{\bar{\eta}+\eta'}\right]\frac{d\bar{\eta}}{\varrho_4}\,, \end{aligned}\right\} \qquad (4.3)$$

with

$$\left.\begin{aligned} \hat{\sigma}_{1,1-\psi}^{\,2} &= (1-\eta'-\psi)^2 + \varepsilon^2(\xi-\xi\eta'+\psi)^2\,, \\ \hat{\sigma}_{2,1-\psi}^{\,2} &= (1-\eta'-\psi)^2 + \varepsilon^2(\xi-\xi\eta'-\psi)^2\,, \\ \hat{\sigma}_{3,1-\psi}^{\,2} &= (1+\eta'-\psi)^2 + \varepsilon^2(\xi-\xi\eta'+\psi)^2\,, \\ \hat{\sigma}_{4,1-\psi}^{\,2} &= (1+\eta'-\psi)^2 + \varepsilon^2(\xi-\xi\eta'-\psi)^2\,. \end{aligned}\right\} \qquad (4.4)$$

The integrals of (4.3) have been evaluated by expanding them into convergent power series as for the whole rhombus, and details of the analysis are given in Appendix III.

If we substitute $\xi = 0$, $\eta' = 0$ in (4.2), (4.3) and (4.4), we get the formula for the *centre* of a cropped-rhombus wing:

$$-\frac{\pi\hat{v}_x}{4U\vartheta} = \frac{\Omega}{4} + \bar{I}_1\,, \qquad (4.5)$$

where

$$\left.\begin{aligned} \Omega &= \frac{1}{\varepsilon}\ln\psi\ln\left[\frac{\varepsilon\psi + \{(1-\psi)^2 + \varepsilon^2\psi^2\}^{1/2}}{-\varepsilon\psi + \{(1-\psi)^2 + \varepsilon^2\psi^2\}^{1/2}}\right], \\ \bar{I}_1 &= \bar{I}_2 = \bar{I}_3 = \bar{I}_4 = -\int_{1-\psi}^{1}\left[1 + \frac{\ln(1-\bar{\eta})}{\bar{\eta}}\right]\frac{d\bar{\eta}}{\varrho_1}\,, \\ \varrho_1^{\,2} &= \bar{\eta}^2 + \varepsilon^2(1-\bar{\eta})^2\,. \end{aligned}\right\} \qquad (4.6)$$

Figs. 4 and 5 show the variation of the supervelocity at the centre of straight tapered wings with ψ and ε. Fig. 5 also shows lines of constant aspect ratio A (*see* formula for A in the footnote under section 2). The values of A when $\psi = 1{\cdot}0$ are obtained directly from the values for rectangular straight wings (*see* Ref. 2, equation 4.2.3 and Fig. 2).

If we put $\xi = 0$ while keeping η' arbitrary in (4.2), (4.3) and (4.4), we get simplified formulae for the *mid-chord line* of the cropped wing:

$$\left.\begin{aligned} -\pi\hat{v}_{x\,r}/2U\vartheta &= \tfrac{1}{2}\Omega + \bar{I}_1\,, \\ -\pi\hat{v}_{x\,l}/2U\vartheta &= \tfrac{1}{2}A + \bar{I}_3\,, \end{aligned}\right\} \qquad \ldots\ \ldots\ \ldots\ \ldots\ \ldots\ \ldots\ \ldots\ \ldots \qquad (4.7)$$

where

$$\left.\begin{aligned} (\Omega)_{\xi=0} &= \frac{1}{\varepsilon}\ln\psi\ln\frac{\varepsilon\psi + [(1-\eta'-\psi)^2 + \varepsilon^2\psi^2]^{1/2}}{-\varepsilon\psi + [(1-\eta'-\psi)^2 + \varepsilon^2\psi^2]^{1/2}}\,, \\ (A)_{\xi=0} &= \frac{1}{\varepsilon}\ln\psi\ln\frac{\varepsilon\psi + [(1+\eta'-\psi)^2 + \varepsilon^2\psi^2]^{1/2}}{-\varepsilon\psi + [(1+\eta'-\psi)^2 + \varepsilon^2\psi^2]^{1/2}}\,, \\ \bar{I}_1 = \bar{I}_2 &= -\int_{1=\psi}^{1}\left\{1 + (1-\eta')\frac{\ln(1-\bar{\eta})}{\bar{\eta}-\eta'}\right\}\frac{d\bar{\eta}}{\varrho_1}\,, \\ \bar{I}_3 = \bar{I}_4 &= -\int_{1=\psi}^{1}\left\{1 + (1+\eta')\frac{\ln(1-\bar{\eta})}{\bar{\eta}+\eta'}\right\}\frac{d\bar{\eta}}{\varrho_3}\,, \end{aligned}\right\} \qquad \ldots\ \ldots\ \ldots \qquad (4.8)$$

the expressions for ϱ_1 and ϱ_3 being now defined by (3.22).

The supervelocity along the mid-chord line of the cropped wing has been computed for values of ψ of $0{\cdot}3$ and $0{\cdot}6$ for values of ε varying from 0 to $1{\cdot}0$. This again gives the local maximum supervelocities across the wing, and it is seen from Figs. 10 and 11 that the effect of cropping the wing is to bring about a considerable reduction of the supervelocity at the tips which drops to roughly half its original value at the same spanwise station. The tip effect for a tapered wing is therefore similar to that for an untapered one. Thus it is clear that the effect of tapering and cropping a wing may be advantageous by comparison with an infinite untapered wing. If comparing with rectangular wings, the effect is more subtle and depends on the choice of the latter. We may, for example, make a comparison for either plan form families of constant s/b or constant aspect ratio A. Fig. 12 shows the variation of the true maximum supervelocities (wherever they occur) for wings of constant s/b or A, the values of either ratio being taken alternatively as $2{\cdot}5$ and $5{\cdot}0$. It should be noticed that the effect of taper is only quite small in all cases but is more marked for the lower values of s/b or A and somewhat more significant when A is kept constant rather than s/b. For moderate to large values of ψ, taper does reduce the maximum to a small extent but, with decreasing ψ, the effect is reversed. If, however, the local maximum supervelocity at the central sections had been compared for these wings this would have indicated a marked beneficial effect from taper which would be quite erroneous. It should be pointed out that only two points on each of the curves of Fig. 12 have been determined accurately (from our Figs. 10 and 11, using interpolation as necessary), apart from the values for the rectangular wings ($\psi = 1$), which have been taken from Ref. 2, Fig. 24, and fully tapered wings ($\psi = 0$) where the values are logarithmically infinite. The reason for this is that our computation of v_x for cropped wings has been made for only two values of $\psi = 0{\cdot}3$ and $0{\cdot}6$. The curves of Fig. 12 do suffice, however, to show the general trend of the effect of taper.

It has been thought justifiable to undertake one more computational effort so as to obtain an illustrative picture of supervelocity distribution over an entire cropped wing. The values of the parameters chosen are $\varepsilon = 0{\cdot}3$ and $\psi = 0{\cdot}3$. The numerical results are given in Table 4, supervelocity diagrams in Fig. 9, and the wing with its isobars is represented in Fig. 14.

The isobar pattern in Fig. 14 may be best examined by comparison with that of Fig. 13 (full rhombus with the same ε). It is seen that the central area presents an almost identical picture in both cases because, obviously, the effect of the distant small tip triangles which have been cut

off is so slight. The pattern changes, however, in the remaining areas near the tips where supervelocities are greatly reduced so that the higher isobars, instead of converging to the imaginary sharp tip, double again back on themselves becoming more or less similar to those in the familiar cases of untapered tip areas (Ref. 2, Fig. 26). As a result, the high isobars become narrow ovals stretched spanwise, separate in each half-wing*. Somewhat lower isobars (with index little below the maximum of the central section, 0·897 in the present case) again cross the central section, thus becoming large ovals extending over both wing halves—there being again a separating isobar of slender ' eight ' shape with a double point at the centre. Even lower isobars, with index below the tip maximum (0·571 in our example) reach the tip section and thus split into two full-span branches of mild curvature. The taper effect dominates the central area, while the tip effect rules two regions of its own.

Fig. 14 is again representative of a wide class of cropped-rhombus wings, but not to such a degree as the typical full rhombus pattern of Fig. 13. In the previous case, only one parameter, ε, affected the picture, resulting in merely quantitative modifications. Now we have to deal with two parameters, ε and ψ, and the pattern may undergo even qualitative changes as either of the two prevails. Thus, as ψ increases the tip effects gradually suppress that of taper even in the central area, producing a pattern more similar to that of untapered plan forms of small aspect ratio. The changes may be predicted approximately by examining the diagrams of supervelocity along the mid-chord line (as in Figs. 10 and 11). It is seen that as the wing is cropped more and more (increasing ψ), the two separated regions of closed ovals enclosing the two ' foci ' in both half-wings become increasingly narrow, the foci themselves receding inboard. The effect is more pronounced at larger ε's so that, *e.g.*, when $\varepsilon = 1$ and $\psi = 0{\cdot}6$, these two regions practically disappear. With even greater ψ, the foci would coalesce at the centre and then the pattern would consist of just ovals over both wing halves, and full-span branches. This, however, will only occur for wings of very small aspect ratio, with no practical significance.

The change of profile will again produce modifications consisting in destroying the fore-and-aft symmetry, usually increasing the maxima and displacing them chord-wise, crowding the isobars where the curvature of the profile increases, etc., but no important qualitative changes are to be expected for well-shaped profiles.

As for critical Mach number, the position is at least fundamentally clear, if not promising as far as actual computation is concerned. The first danger points in most cases (at least for profiles with fore-and-aft symmetry) will obviously be the two ' foci ', and these will determine the ' lower criticals ' for the wing. Shock-waves, once started near the foci, will then spread both inboard and outboard as the speed increases, the central area being reached quite soon. Only in cases of large values of both ε and ψ will the root section be relevant for the lower critical when shock-waves will gradually spread outboard from the centre towards both tips. The calculation would be troublesome as, in compressible flow, the Göthert's three-dimensional paraphrase of the Glauert-Prandtl law would have to be applied so that, for each Mach number an ' analogous ' wing with span and thickness reduced to the $\sqrt{(1 - M^2)}$ fraction of their original values would have to be considered, the thickness ratio remaining spanwise constant, however. Diagrams as those of Figs. 10 and 11 would be needed, and the calculations would proceed on the lines of Ref. 6. It is not proposed to enlarge on the subject here, but it may be mentioned that, according to the results of this paper as to maximum supervelocities, no considerable benefits are to be expected for tapered wings as against untapered ones unless the aspect ratio is particularly small. In practice, small aspect ratio wings will usually be strongly swept-back leading to delta plan forms, and in such cases one more effort will be needed to overcome the combined theoretical difficulties of sweepback and taper. Even when the wing plan form has fore-and-aft symmetry but its profile has not, some aspects of sweepback play a part because the highest isobars then run obliquely to the main flow.

---

* And enclosing respectively, the two ' foci ' with supervelocities maximum for the entire wing area (index 0·994 in our case).

LIST OF SYMBOLS

Explanation of Typographical Signs and Suffixes.—The suffixes r, l refer to the right-hand and left-hand sides of the wing respectively.

The suffixes L, T refer to the leading and trailing edges of the wing.

The suffix $_0$ when used with φ refers to the mid-chord line.

The suffixes 1, 2, 3, 4 for the square roots (r, ϱ, R) indicate the integrals in which they occur, for instance r_1 occurs in I_1, etc. The irrational factors of the square roots with limits substituted (σ's) have two suffixes, the first indicating the integral in which they occur and the second suffix (0, 1, 2 or 1 — ψ) indicating the upper or lower limit of integration which has been substituted.

A similar system has been used for the series of I's and T's (*see* Appendices). The first suffix refers to the integral of which the series is part (I_1, I_2, etc.), and the second is the number of the term in the power series. Thus $I_{1\,m}$ is the m^{th} term of the power series of I's in I_1. Similarly for $T_{1\,m}$, etc.

For the rhombus wing I_1 and I_2 are expanded in a different way over the outboard part of the semi-span, and I_1 and I_2 are split up into several integrals which are denoted by the additional suffixes h, j, k, p. The terms in the power series in these integrals (where it was necessary to expand in such series) therefore have three suffixes: the third indicating now the number of the term in the series. For example, $T_{1\,h\,m}$ is the m^{th} term in the power series in the integral $I_{1\,h}$ (the h-part integral of I_1).

The suffixes 1, 0, (1 — ψ) used with the auxiliary variables μ, ν, τ denote the values of these variables at the upper and lower limits of integration.

In the expansion of the I's there are symbols of the form $I_{1\,-1}$, $I_{1\,0}$, etc.; the second suffix in these cases indicates the power of the variable (such as μ, ν, τ) in the numerator of the integral. For instance:

$$I_{1\,-1} = \int_{\mu_0}^{\mu_1} \frac{d\mu}{\mu R_1}, \qquad I_{1\,0} = \int_{\mu_0}^{\mu_1} \frac{d\mu}{R_1}.$$

The sign $\hat{}$ over a symbol indicates the values for the cut-off tips of a cropped wing and the supervelocities thus marked must be subtracted from those corresponding to the fully tapered wing.

A	Aspect ratio
a_3, a_4, etc.	Constants, *see* (II.43), (II.44)
b	Semi-root chord
c	Chord at any spanwise station (variable owing to taper)
c_r	Root chord
c_t	Tip chord
$F(x,y)$	Function determining wing surface or, for a fixed y, profile at any spanwise station, *see* (2.2)
f	Function determining the contribution of right-hand half-wing to v_x in terms of dimensional co-ordinates x, y, *see* (3.9)
g	Function determining the contribution of right-hand half-wing to v_x in terms of non-dimensional co-ordinates ξ, η', *see* (3.11)
I	Integrals appearing in the solution Carries appropriate suffixes.

l		Distance QP, *see* Figs. 1, 2, 3
m		Index denoting arbitrary term in an infinite series
P		Terms of the power series of inverse square root occurring in the solution, *see* (II.47) Carries appropriate suffixes
q		Source strength per unit area, *see* (2.1) and (2.3)
R		Various non-dimensional expressions in μ, ν, τ defined by (I.10) (II.5), (II.52) and (III.6) Carries appropriate suffixes
r		Various dimensional expressions in x and y defined by (3.5) and (I.3) Carries appropriate suffixes
S		Wing area
s		Wing semi-span
s'		Distance of point of intersection of wing leading and trailing edges from the root chord (this is equal to s for fully tapered wings)
T		Terms of the power series of logarithms occurring in the solution, *see* Appendices Carries appropriate suffixes
t	$=$	$-\mu$ Auxiliary variable, *see* (II.43)
U		Undisturbed velocity of the air flow
v_x, v_y		Components of induced velocity Carries appropriate suffixes
x, y		Chordwise and spanwise co-ordinates
$\bar{x}$, $\bar{y}$		Chordwise and spanwise co-ordinates of a source element, being fundamental variables of integration
$\bar{x}_L$, $\bar{x}_T$		Values of $\bar{x}$ at the limits of integration, *i.e.*, at leading or trailing edge
z		Vertical co-ordinate
β		Angle, *see* Figs. 1, 2, 3
ε	$=$	b/s' Coefficient of convergence
η'	$=$	y/s' Non-dimensional spanwise co-ordinate of a point on the right-hand part of the wing surface
$\bar{\eta}$		Similar co-ordinate for a chordwise source-and-sink strip
ϑ		Thickness ratio of wing profile
Λ		Portmanteau symbol, *see* (4.3)
μ		Auxiliary variable, defined by (II.3) or, in the particular case of the central section, by (I.8)
ν		Auxiliary variable defined by (I.8)
ξ	$=$	$\dfrac{x + y \tan \varphi_0}{b(1 - \eta')}$ Non-dimensional chordwise co-ordinate of a point on the right-hand part of the wing surface

LIST OF SYMBOLS—*continued*

ϱ Various expressions in $\bar{\eta}$, η' and ξ, defined alternatively by (3.8), (3.15), (3.22), (4.6)
Carries appropriate suffixes

σ Various expressions in η' and ξ obtained from R after substitution of limits of integration, defined alternatively by (I.17), (I.31), (II.15), (II.30), (II.58), (III.12), (III.28)
Carries appropriate suffixes

τ Auxiliary variable defined by (II.50)

φ Angle of sweepback
Carries appropriate suffixes

$\psi = c_t/c_r$ Taper ratio of wing

Ω Portmanteau symbol, *see* (4.3)

REFERENCES

No.	*Author*	*Title, etc.*
1	S. Neumark	Velocity Distribution on Straight and Swept-back Wings of Small Thickness and Infinite Aspect Ratio at Zero Incidence. R. & M. 2713. May, 1947.
2	S. Neumark and J. Collingbourne ..	Velocity Distribution on Untapered Sheared and Swept-back Wings of Small Thickness and Finite Aspect Ratio at Zero Incidence. R. & M. 2717. March, 1949.
3	S. Neumark	Critical Mach Numbers for Thin Untapered Swept Wings at Zero Incidence. R. & M. 2821. November, 1949.
4	H. H. B. M. Thomas	Definitions for Swept Wings. R.A.E. Tech. Memo. No. Aero. 168. March, 1951.
5	C. H. E. Warren	Wing Planforms for Systematic Tests. R.A.E. Tech. Memo. No. Aero. 171. March, 1951.
6	S. Neumark	Critical Mach Numbers for Swept-back Wings. Paper presented to Section 2, VIIth International Congress of Applied Mechanics, London, September, 1948, and published in *The Aeronautical Quarterly* of the *R.Ae.S.*, Vol. II. August, 1950.
7	J. Edwards	*A Treatise on the Integral Calculus*. Macmillan and Co., London. Vol. I. 1930.
8	A. Fiul	Finite Wings at Zero Lift in Subsonic Flow. Northrop Aircraft Inc. Report No. R.A.16. June, 1948.

APPENDIX I (To Section 2)

Velocity Distribution at the Central Section of a Fully Tapered Swept-back Wing with Biconvex Parabolic Profile and Spanwise Constant Thickness Ratio

In the following calculations the chordwise integration is performed before the spanwise and η' is equated to zero before the integration. The results thus obtained have been checked with the formula for an infinite swept-back wing by finding the limiting value when the convergence ratio ε tends to zero.

The general formula for the supervelocity at *any point on the surface* of a swept-back fully tapered wing (angle of sweepback of the mid-chord line φ_0, coefficient of convergence ε, and taper ratio $\psi = 0$, *see* Fig. 2) is found by substituting the first and second derivatives of (2.8), with respect to x, in the general formula (2.7). Hence, for the right-hand half-wing:

$$\frac{\pi v_{xr}}{U\vartheta} = \int_0^{s'} \left[\left| \frac{\bar{x} + \bar{y}\tan\varphi_0}{b(1-\bar{y}/s')\,[(x-\bar{x})^2 + (y-\bar{y})^2]^{1/2}} \right|_{\bar{x}_T}^{\bar{x}_L} - \frac{1}{b(1-\bar{y}/s')} \int_{\bar{x}_T}^{\bar{x}_L} \frac{d\bar{x}}{[(x-\bar{x})^2 + (y-\bar{y})^2]^{1/2}} \right] d\bar{y} \quad .. \quad .. \quad .. \quad \text{(I.1)}$$

or

$$\frac{\pi v_{xr}}{U\vartheta} = \int_0^{s'} \left[\frac{1}{r_1} + \frac{1}{r_2} + \frac{1}{b(1-\bar{y}/s')} \ln\left(\frac{x - b + \bar{y}\tan\varphi_L + r_2}{x + b + \bar{y}\tan\varphi_T + r_1} \right) \right] d\bar{y}\,, \quad .. \quad .. \quad .. \quad \text{(I.2)}$$

where the limits of integration $\bar{x}_T$, $\bar{x}_L$ are defined in (2.6) and

$$\left.\begin{aligned} r_1^2 &= (x + b + \bar{y}\tan\varphi_T)^2 + (y-\bar{y})^2\,, \\ r_2^2 &= (x - b + \bar{y}\tan\varphi_L)^2 + (y-\bar{y})^2\,. \end{aligned}\right\} \quad .. \quad .. \quad .. \quad .. \quad .. \quad .. \quad \text{(I.3)}$$

If we now put $y = 0$ in (I.2), we then obtain the *supervelocity in the central section induced by the right-hand half-wing*, which may be written in non-dimensional form:

$$\frac{\pi v_{xr}}{U\vartheta} = \int_0^1 \frac{d\bar{\eta}}{\varrho_1} + \int_0^1 \frac{d\bar{\eta}}{\varrho_2} + \frac{1}{\varepsilon}\int_0^1 \ln\left(\frac{\bar{\eta}\tan\varphi_L - \varepsilon(1-\xi) + \varrho_2}{\bar{\eta}\tan\varphi_T + \varepsilon(1+\xi) + \varrho_1} \right) \frac{d\bar{\eta}}{1-\bar{\eta}}\,, \quad .. \quad .. \quad .. \quad \text{(I.4)}$$

where

$$\left.\begin{aligned} \varrho_1^2 &= \bar{\eta}^2\sec^2\varphi_T + 2\varepsilon(1+\xi)\bar{\eta}\tan\varphi_T + \varepsilon^2(1+\xi)^2\,, \\ \varrho_2^2 &= \bar{\eta}^2\sec^2\varphi_L - 2\varepsilon(1-\xi)\bar{\eta}\tan\varphi_L + \varepsilon^2(1-\xi)^2\,. \end{aligned}\right\} \quad .. \quad .. \quad .. \quad .. \quad \text{(I.5)}$$

The *contribution of the left-hand half-wing* will be exactly the same, owing to symmetry.

Integrating the logarithmic term in (I.4) by parts, and substituting the limits, where possible, we may present the formula for the *total supervelocity in the central section* in the form:

$$-\pi v_x/2U\vartheta = I_1 + I_2\,, \quad .. \quad .. \quad .. \quad .. \quad .. \quad .. \quad .. \quad .. \quad .. \quad \text{(I.6)}$$

with

$$\left.\begin{aligned} I_1 &= -\int_0^1 \left(1 + (1+\xi)\frac{\ln(1-\bar{\eta})}{\bar{\eta}} \right) \frac{d\bar{\eta}}{\varrho_1}\,, \\ I_2 &= -\int_0^1 \left(1 + (1-\xi)\frac{\ln(1-\bar{\eta})}{\bar{\eta}} \right) \frac{d\bar{\eta}}{\varrho_2}\,. \end{aligned}\right\} \quad .. \quad .. \quad .. \quad .. \quad \text{(I.7)}$$

The formula (I.6) applies for an arbitrary value of ε, but it would not be permissible to let $\varepsilon \to 0$ at this stage. This will only be possible after the following transformation.

Neither of the integrals, (I.7), can be evaluated in terms of simple transcendents or tabulated functions, so it has been decided to expand the logarithms in power series and integrate term by term for a sufficient number of terms to give the required accuracy. Before doing this, however, the variables of integration have been changed in an analogous way to that which will be used for the rhombus wing (*see* Appendix II).

Introducing the *auxiliary variables* defined by

$$\left.\begin{aligned} \mu &= \bar{\eta}/(1+\xi) \\ \nu &= \bar{\eta}/(1-\xi) \end{aligned}\right\} \quad .. \quad .. \quad .. \quad .. \quad .. \quad .. \quad .. \quad .. \quad \text{(I.8)}$$

for I_1 and I_2, respectively, we obtain :

$$\left.\begin{aligned} I_1 &= -\cos\varphi_T \int_0^{1/1+\xi} \left[1+\frac{1}{\mu}\ln\{1-\mu(1+\xi)\}\right]\frac{d\mu}{R_1}, \\ I_2 &= -\cos\varphi_L \int_0^{1/1-\xi} \left[1+\frac{1}{\nu}\ln\{1-\nu(1-\xi)\}\right]\frac{d\nu}{R_2}; \end{aligned}\right\} \quad .. \quad .. \quad .. \quad \text{(I.9)}$$

where

$$\left.\begin{aligned} R_1^2 &= \mu^2 + 2\varepsilon\mu\sin\varphi_T\cos\varphi_T + \varepsilon^2\cos^2\varphi_T, \\ R_2^2 &= \nu^2 - 2\varepsilon\nu\sin\varphi_L\cos\varphi_L + \varepsilon^2\cos^2\varphi_L. \end{aligned}\right\} \quad .. \quad .. \quad .. \quad .. \quad \text{(I.10)}$$

Let us consider I_1. Expanding the logarithm in a *power series* (valid throughout the range of integration), we obtain:

$$I_1 = \cos\varphi_T \int_0^{1/1+\xi} \left[\xi + \tfrac{1}{2}\mu(1+\xi)^2 + \tfrac{1}{3}\mu^2(1+\xi)^3 + \ldots\right]\frac{d\mu}{R_1}, \quad .. \quad .. \quad \text{(I.11)}$$

or

$$I_1 = \xi I_{1\,0}\cos\varphi_T + (1+\xi)^2\cos\varphi_T\left[\tfrac{1}{2}I_{1\,1} + \tfrac{1}{3}(1+\xi)I_{1\,2} + \tfrac{1}{4}(1+\xi)^2 I_{1\,3} + \ldots\right] \quad .. \quad .. \quad .. \quad \text{(I.12)}$$

where

$$I_{1\,m} = \int_0^{1/1+\xi} \frac{\mu^m}{R_1}\,d\mu, \quad .. \quad .. \quad .. \quad .. \quad .. \quad .. \quad .. \quad .. \quad \text{(I.13)}$$

and hence

$$I_{1\,0} = \int_0^{1/1+\xi} \frac{d\mu}{R_1} = \ln\left(\frac{1+\varepsilon(1+\xi)\sin\varphi_T\cos\varphi_T + \sigma_{1\,1}}{\varepsilon(1+\xi)(1+\sin\varphi_T)\cos\varphi_T}\right), \quad .. \quad .. \quad .. \quad \text{(I.14)}$$

$$I_{1\,1} = \frac{\sigma_{1\,1}}{1+\xi} - \varepsilon\cos\varphi_T - \varepsilon I_{1\,0}\sin\varphi_T\cos\varphi_T, \quad .. \quad .. \quad .. \quad .. \quad \text{(I.15)}$$

$$I_{1\,2} = \frac{[1-3\varepsilon(1+\xi)\sin\varphi_T\cos\varphi_T]\sigma_{1\,1}}{2(1+\xi)^2} + \frac{3\varepsilon^2\sin\varphi_T\cos^2\varphi_T}{2} - \frac{\varepsilon^2(1-3\sin^2\varphi_T)I_{1\,0}\cos^2\varphi_T}{2}, \quad .. \quad .. \quad .. \quad .. \quad .. \quad \text{(I.16)}$$

and ${\sigma_{1\,1}}^2$ is a factor appearing in the expression for R_1^2, obtained after substituting the upper limit of integration:

$${\sigma_{1\,1}}^2 = 1 + 2\varepsilon(1+\xi)\sin\varphi_T\cos\varphi_T + \varepsilon^2(1+\xi)^2\cos^2\varphi_T. \quad .. \quad .. \quad .. \quad \text{(I.17)}$$

It has been found that the series $\sum_1^\infty I_{1\,m}$ is not rapidly convergent, and so another series—that which is formed when $\varepsilon \to 0$ in $I_{1\,1}$, $I_{1\,2}$, etc.—is combined with it in such a way as to produce one series whose sum to infinity is known and another which is quite rapidly convergent.

As $\varepsilon \to 0$, $I_{1\,1} \to 1/1 + \xi$, $I_{1\,2} \to \frac{1}{2}/(1 + \xi)^2$, etc., and hence:

$$I_1 = I_{1\,0}\,\xi \cos \varphi_T + \sum_{m=1}^{\infty} \frac{(1 + \xi)^{m+1}}{(m + 1)m} \left[\frac{1}{(1 + \xi)^m} - \left(\frac{1}{(1 + \xi)^m} - m I_{1\,m} \frac{\cos \varphi_T}{\cos \varphi_0} \right) \right] \cos \varphi_0 \quad .. \quad \text{(I.18)}$$

or

$$I_1 = I_{1\,0}\,\xi \cos \varphi_T + (1 + \xi) \left[\sum_1^{\infty} \frac{1}{(m + 1)m} - \sum_1^{\infty} T_{1\,m} \right] \cos \varphi_0 , \quad .. \quad \text{(I.19)}$$

or, *finally*:

$$I_1 = I_{1\,0}\,\xi \cos \varphi_T + (1 + \xi) \left(1 - \sum_1^{\infty} T_{1\,m} \right) \cos \varphi_0 , \quad .. \quad .. \quad .. \quad \text{(I.20)}$$

where

$$T_{1\,m} = \frac{1}{(m + 1)m} - \frac{(1 + \xi)^m I_{1\,m}}{m + 1} \frac{\cos \varphi_T}{\cos \varphi_0} . \quad .. \quad .. \quad .. \quad .. \quad .. \quad \text{(I.21)}$$

For the computation a recurrence formula for $T_{1\,m}$ was used. Edwards[7], on page 235, paragraph 240, gives the following relationship:

$$x^{m-1} (a + bx + cx^2)^{1/2} = (m - 1)a \int \frac{x^{m-2}}{(a + bx + cx^2)^{1/2}}\, dx + \tfrac{1}{2}(2m - 1)b \int \frac{x^{m-1}}{(a + bx + cx^2)^{1/2}}\, dx + mc \int \frac{x^m}{(a + bx + cx^2)^{1/2}}\, dx \ldots \quad \text{(I.22)}$$

From this formula we get:

$$I_{1\,m} = \frac{\sigma_{1\,1}}{m(1 + \xi)^m} - \frac{m - 1}{m} I_{1\,m-2}\, \varepsilon^2 \cos^2 \varphi_T - \frac{2m - 1}{m} I_{1\,m-1}\, \varepsilon \sin \varphi_T \cos \varphi_T , \quad \text{(I.23)}$$

and substituting for $I_{1\,m}$ from (I.20) in (I.23):

$$T_{1\,m} = \frac{1}{(m + 1)m} \left[1 - \sigma_{1\,1} \frac{\cos \varphi_T}{\cos \varphi_0} \right] + \frac{\varepsilon(1 + \xi) \cos \varphi_T}{m + 1} \left[\frac{(m - 1)^2 \varepsilon(1 + \xi) \cos \varphi_T + (2m - 1)(m - 2) \sin \varphi_T}{m(m - 1)(m - 2)} - \frac{(m - 1)^2}{m} \varepsilon(1 + \xi) T_{1\,m-2} \cos \varphi_T - (2m - 1) T_{1\,m-1} \sin \varphi_T \right] . \quad .. \quad .. \quad \text{(I.24)}$$

This recurrence formula can be used for all values of m greater than 2, but $T_{1\,1}$ and $T_{1\,2}$ must be found from (I.15), (I.16) and (I.21):

$$T_{1\,1} = \frac{1}{2} \left[1 - \sigma_{1\,1} \frac{\cos \varphi_T}{\cos \varphi_0} + \varepsilon(1 + \xi) \frac{\cos^2 \varphi_T}{\cos \varphi_0} + I_{1\,0}\, \varepsilon(1 + \xi) \frac{\cos^2 \varphi_T}{\cos \varphi_0} \sin \varphi_T \right] , \quad .. \quad \text{(I.25)}$$

$$T_{1\,2} = \frac{1}{6} \left[1 - \sigma_{1\,1} \{1 - 3\varepsilon(1 + \xi) \sin \varphi_T \cos \varphi_T\} \frac{\cos \varphi_T}{\cos \varphi_0} - 3\varepsilon^2(1 + \xi) \frac{\cos^3 \varphi_T}{\cos \varphi_0} \sin \varphi_T + I_{1\,0}\, \varepsilon^2(1 + \xi)^2 (1 - 3 \sin^2 \varphi_T) \frac{\cos^3 \varphi_T}{\cos \varphi_0} \right] . \quad .. \quad \text{(I.26)}$$

The corresponding formulae for I_2 are found by replacing ξ by $(-\xi)$ and φ_T by $(-\varphi_L)$, then

$$I_2 = - I_{2\,0}\, \xi \cos \varphi_L + (1 - \xi)\left(1 - \sum_1^{\infty} T_{2\,m}\right) \cos \varphi_0 \quad .. \quad .. \quad .. \quad .. \quad .. \quad \text{(I.27)}$$

where

$$I_{2\,0} = \ln \left[\frac{1 - \varepsilon(1 - \xi) \sin \varphi_L \cos \varphi_L + \sigma_{2\,1}}{\varepsilon(1 - \xi)(1 - \sin \varphi_L) \cos \varphi_L} \right] , \quad .. \quad .. \quad .. \quad .. \quad .. \quad \text{(I.28)}$$

$$T_{2\,1} = \frac{1}{2}\left[1 - \sigma_{2\,1}\frac{\cos\varphi_L}{\cos\varphi_0} + \varepsilon(1-\xi)\frac{\cos^2\varphi_L}{\cos\varphi_0} - I_{2\,0}\,\varepsilon(1-\xi)\frac{\cos^2\varphi_L}{\cos\varphi_0}\sin\varphi_L\right], \quad .. \quad \text{(I.29)}$$

and

$$T_{2\,2} = \frac{1}{6}\left[1 - \sigma_{2\,1}\{1 + 3\varepsilon(1-\xi)\sin\varphi_L\cos\varphi_L\}\frac{\cos\varphi_L}{\cos\varphi_0}\right.$$
$$\left. + 3\varepsilon^2(1-\xi)^2\frac{\cos^3\varphi_L}{\cos\varphi_0}\sin\varphi_L + I_{2\,0}\,\varepsilon^2(1-\xi)^2(1-3\sin^2\varphi_L)\frac{\cos^3\varphi_L}{\cos\varphi_0}\right], \quad .. \quad \text{(I.30)}$$

where

$$\sigma_{2\,1}{}^2 = 1 - 2\varepsilon(1-\xi)\sin\varphi_L\cos\varphi_L + \varepsilon^2(1-\xi)^2\cos^2\varphi_L\,. \quad .. \quad .. \quad .. \quad .. \quad \text{(I.31)}$$

The recurrence formula for $T_{2\,m}$ is then:

$$T_{2\,m} = \frac{1}{(m+1)m}\left(1 - \sigma_{2\,1}\frac{\cos\varphi_L}{\cos\varphi_0}\right)$$
$$+ \frac{\varepsilon(1-\xi)\cos\varphi_L}{m+1}\left(\frac{(m-1)^2\varepsilon(1-\xi)\cos\varphi_L - (2m-1)(m-2)\sin\varphi_L}{m(m-1)(m-2)}\right.$$
$$\left. - \frac{(m-1)^2}{m}\varepsilon(1-\xi)\,T_{2,\,m-2}\cos\varphi_L + (2m-1)T_{2,\,m-1}\sin\varphi_L\right). \quad .. \quad .. \quad \text{(I.32)}$$

Adding (I.20) and (I.27), we obtain the *total supervelocity* at the central section:

$$-\pi v_x/2U\vartheta = \left[2 - (1-\xi)\sum_1^\infty T_{2\,m} - (1+\xi)\sum_1^\infty T_{1\,m}\right]\cos\varphi_0$$
$$- \xi(I_{2\,0}\cos\varphi_L - I_{1\,0}\cos\varphi_T)\,. \quad .. \quad .. \quad .. \quad .. \quad .. \quad .. \quad \text{(I.33)}$$

The above formulae give now all that is needed for computing v_x in any particular case, but no attempts at this have been made thus far.

Let us now consider the *limiting case* $\varepsilon \to 0$. Then $I_{1\,m} \to 1/m(1+\xi)^m$ and $\varphi_L = \varphi_0 = \varphi_T = \varphi$; therefore, from (I.21), we find that all $T_{1\,m} \to 0$. Similarly $T_{2\,m}$ tends to zero for any value of m from 1 to ∞, and (I.33) therefore reduces to:

$$-\frac{\pi v_x}{4U\vartheta\cos\varphi} = 1 - \tfrac{1}{2}\xi\lim_{\varepsilon\to 0}(I_{2\,0} - I_{1\,0})\,. \quad .. \quad .. \quad .. \quad .. \quad .. \quad .. \quad \text{(I.34)}$$

Now

$$I_{2\,0} - I_{1\,0} = \ln\left(\frac{1 - \varepsilon(1-\xi)\sin\varphi_L\cos\varphi_L + \sigma_{2\,1}}{1 + \varepsilon(1+\xi)\sin\varphi_T\cos\varphi_T + \sigma_{1\,1}}\,\frac{(1+\xi)(1+\sin\varphi_T)\cos\varphi_T}{(1-\xi)(1-\sin\varphi_L)\cos\varphi_L}\right), \quad .. \quad \text{(I.35)}$$

and the limit of (I.35) when ε tends to zero is:

$$\lim_{\varepsilon\to 0}(I_{2\,0} - I_{1\,0}) = \ln\left[\frac{1+\xi}{1-\xi}\,\frac{1+\sin\varphi}{1+\sin\varphi}\right], \quad .. \quad .. \quad .. \quad .. \quad .. \quad \text{(I.36)}$$

where $\varphi_L = \varphi_T = \varphi$.

The supervelocity distribution at the central section of an infinite swept-back wing of constant chord with biconvex parabolic profile is therefore:

$$-\pi v_x/4U\vartheta = \left[1 - \tfrac{1}{2}\xi\ln\left\{\frac{1+\xi}{1-\xi}\,\frac{1+\sin\varphi}{1-\sin\varphi}\right\}\right]\cos\varphi\,, \quad .. \quad .. \quad .. \quad .. \quad \text{(I.37)}$$

which is as given in Ref. 1, formula (6.1). This result seems to indicate that performing the chordwise integration before the spanwise may often be preferred to the reverse order, as, even when y is put equal to zero before integrating, the results for the central section come out correct. In the case of a tapered wing, this order of integration is certainly the only appropriate one and has therefore been used throughout.

APPENDIX II (To Section 3)

Velocity Distribution over the Entire Surface of a Rhombus Wing with Biconvex Parabolic Profile and Spanwise Constant Thickness Ratio

The velocity distribution over a full-rhombus wing (where $\varphi_0 = 0$, $\psi = 0$) is given by (3.16):

$$\left.\begin{aligned} &\text{contribution of right-hand half wing} - \pi v_{x\,r}/U\vartheta = I_1 + I_2\,, \\ &\text{contribution of left-hand half-wing} - \pi v_{x\,l}/U\vartheta = I_3 + I_4\,, \end{aligned}\right\} \quad .. \quad .. \quad .. \quad \text{(II.1)}$$

where I_1, I_2, I_3, I_4 are defined by (3.17).

We shall now transform these integrals so as to make them computable. It may be mentioned that in preparing this report, we started with the simplest case of the wing centre (where $I_1 = I_2 = I_3 = I_4$, and this one integral which has to be evaluated is very simple by comparison with the general case). We then considered the special cases of the central section ($I_1 = I_3$, $I_2 = I_4$) and the mid-chord line ($I_1 = I_2$, $I_3 = I_4$); in both these latter cases only two integrals have to be calculated and the results doubled to give the supervelocity. Finally, the general case was investigated. In such a way it was possible to check the results at each stage.

In the following calculations, however, the general case for arbitrary values of η' and ξ (entire wing surface) is investigated, and the transformation is rather long and complicated. However, for the special cases of the central section, mid-chord line and wing centre, the values $\eta' = 0$ and/or $\xi = 0$ should merely be substituted in the final formulae (which are thereby greatly simplified); this will often be all that is necessary.

(A) *Contribution of the Right-hand Half-wing.*—Let us consider

$$I_1 = -\int_0^1 \left\{ 1 + (1+\xi)(1-\eta')\frac{\ln(1-\bar{\eta})}{\bar{\eta}-\eta'} \right\} \frac{d\bar{\eta}}{\varrho_1}\,. \quad .. \quad .. \quad .. \quad .. \quad \text{(II.2)}$$

Introducing an *auxiliary variable*

$$\mu = \frac{\bar{\eta}-\eta'}{(1+\xi)(1-\eta')}\,, \quad .. \quad .. \quad .. \quad .. \quad .. \quad .. \quad .. \quad .. \quad \text{(II.3)}$$

I_1 may be written in a more convenient way:

$$I_1 = -\int_{\mu_0}^{\mu_1} \left\{ 1 + \frac{1}{\mu}\ln(1-\eta') + \frac{1}{\mu}\ln[1-\mu(1+\xi)] \right\} \frac{d\mu}{R_1(1+\varepsilon^2)^{1/2}} \quad .. \quad \text{(II.4)}$$

where

$$R_1^2 = \mu^2 - 2\frac{\varepsilon^2}{1+\varepsilon^2}\mu + \frac{\varepsilon^2}{1+\varepsilon^2}\,, \quad .. \quad .. \quad .. \quad .. \quad .. \quad .. \quad \text{(II.5)}$$

which is much simpler than ϱ_1^2, and the lower and upper limits of integration become:

$$\left.\begin{aligned} \mu_0 &= -\eta'/(1-\eta')(1+\xi)\,, \\ \mu_1 &= 1/(1+\xi)\,. \end{aligned}\right\} \quad .. \quad .. \quad .. \quad .. \quad .. \quad .. \quad .. \quad \text{(II.6)}$$

The power expansion of $\ln[1-\mu(1+\xi)]$ is not valid over the entire span for, when $\eta' > 0{\cdot}5$, $\mu_0(1+\xi) < -1$. If, however, we consider first the *inner part of the semi-span* ($0 \leqslant \eta' < 0{\cdot}5$), then:

$$I_1 = \int_{\mu_0}^{\mu_1} \left[\xi - \frac{1}{\mu}\ln(1-\eta') + \tfrac{1}{2}\mu(1+\xi)^2 + \tfrac{1}{3}\mu(1+\xi)^3 + \ldots \right] \frac{d\mu}{R_1(1+\varepsilon^2)^{1/2}}\,, \quad \text{(II.7)}$$

or

$$I_1 = \frac{1}{(1+\varepsilon^2)^{1/2}} \left[I_{1\,0}\,\xi - I_{1\,-1}\ln(1-\eta') + \sum_{m=1}^{\infty} \left(\frac{(1+\xi)^{m+1}}{m+1} I_{1\,m} \right) \right], \quad .. \quad \text{(II.8)}$$

where the particular terms are defined (for m from -1 to $+\infty$) by:

$$I_{1\,m} = \int_{\mu_0}^{\mu_1} \frac{\mu^m}{R_1}\, d\mu\,; \qquad \text{(II.9)}$$

then the first four of these become:

$$I_{1\,-1} = \int_{\mu_0}^{\mu_1} \frac{d\mu}{\mu R_1} = \left| -\frac{(1+\varepsilon^2)^{1/2}}{\varepsilon} \ln \frac{\varepsilon - \varepsilon\mu + R_1(1+\varepsilon^2)^{1/2}}{|\mu|} \right|_{\mu_0}^{\mu_1}, \qquad \text{(II.10)}$$

or

$$I_{1\,-1} = \frac{(1+\varepsilon^2)^{1/2}}{\varepsilon} \ln \frac{\varepsilon + \varepsilon\xi(1-\eta') + \sigma_{1\,0}}{\eta'(\varepsilon\xi + \sigma_{1\,1})}, \qquad \text{(II.11)}$$

and

$$I_{1\,0} = \int_{\mu_0}^{\mu_1} \frac{d\mu}{R_1} = \ln \frac{(1-\eta')\{1 - \varepsilon^2\xi + \sigma_{1\,1}(1+\varepsilon^2)^{1/2}\}}{-\eta' - \varepsilon^2 - \varepsilon^2\xi(1-\eta') + \sigma_{1\,0}(1+\varepsilon^2)^{1/2}}, \qquad \text{(II.12)}$$

$$I_{1\,1} = \int_{\mu_0}^{\mu_1} \frac{\mu\, d\mu}{R_1} = \frac{(1-\eta')\sigma_{1\,1} - \sigma_{1\,0}}{(1-\eta')(1+\xi)(1+\varepsilon^2)^{1/2}} + \frac{\varepsilon^2}{1+\varepsilon^2} I_{1\,0}, \qquad \text{(II.13)}$$

$$I_{1\,2} = \int_{\mu_0}^{\mu_1} \frac{\mu^2}{R_1}\, d\mu = \frac{(1+4\varepsilon^2+3\varepsilon^2\xi)\sigma_{1\,1}}{2(1+\xi)^2(1+\varepsilon^2)^{3/2}}$$

$$+ \frac{\{\eta'(1+4\varepsilon^2) - 3\varepsilon^2 - 3\varepsilon^2\xi(1-\eta')\}\sigma_{1\,0}}{2(1-\eta')^2(1+\xi)^2(1+\varepsilon^2)^{3/2}} - \frac{\varepsilon^2(1-2\varepsilon^2)}{2(1+\varepsilon^2)^2} I_{1\,0}. \qquad \text{(II.14)}$$

${\sigma_{1\,0}}^2$, ${\sigma_{1\,1}}^2$ are the following factors appearing in the expressions for ${R_1}^2$ obtained after substituting the lower and upper limits of integration, respectively :

$$\left.\begin{aligned} {\sigma_{1\,0}}^2 &= \eta'^2 + \varepsilon^2\{1 + \xi(1-\eta')\}^2, \\ {\sigma_{1\,1}}^2 &= 1 + \varepsilon^2\xi^2. \end{aligned}\right\} \qquad \text{(II.15)}$$

As in the case considered in Appendix I, the series $\sum_1^\infty \left\{ \frac{(1+\xi)^{m+1}}{m+1} \cdot I_{1\,m} \right\}$ is found to be rather slowly convergent, but the difficulty may be overcome by introducing another series whose terms are obtained by putting $\varepsilon = 0$ in $I_{1\,1}$, $I_{1\,2}$, etc., thus:

$$\left.\begin{aligned} (I_{1\,1})_{\varepsilon=0} &= \frac{1}{1+\xi}\left(1 - \frac{\eta'}{1-\eta'}\right), \\ (I_{1\,2})_{\varepsilon=0} &= \frac{1}{2}\frac{1}{(1+\xi)^2}\left[1 + \left(\frac{\eta'}{1-\eta'}\right)^2\right], \text{ etc.}; \end{aligned}\right\} \qquad \text{(II.16)}$$

I_1 may therefore be written as follows:

$$I_1 = \frac{1}{(1+\varepsilon^2)^{1/2}}\left[I_{1\,0}\,\xi - I_{1\,-1}\ln(1-\eta')\right] + \sum_1^\infty \frac{(1+\xi)^{m+1}}{(m+1)m}\left[\frac{1 + (-1)^m\left(\frac{\eta'}{1-\eta'}\right)^m}{(1+\xi)^m}\right.$$

$$\left. - \left\{\frac{1 + (-1)^m\left(\frac{\eta'}{1-\eta'}\right)^m}{(1+\xi)^m} - \frac{mI_{1\,m}}{(1+\varepsilon^2)^{1/2}}\right\}\right], \qquad \text{(II.17)}$$

or

$$I_1 = \frac{1}{(1+\varepsilon^2)^{1/2}}\left[I_{1\,0}\,\xi - I_{1\,-1}\ln(1-\eta')\right] + (1+\xi)\left[\sum_1^\infty \frac{1}{(m+1)m}\right.$$
$$\left. - \sum_1^\infty \left\{(-1)^{m+1}\left(\frac{\eta'}{1-\eta'}\right)^m \cdot \frac{1}{(m+1)m}\right\} - \sum_1^\infty T_{1\,m}\right], \quad .. \quad .. \quad \text{(II.18)}$$

where

$$T_{1\,m} = \frac{1+(-1)^m\left(\frac{\eta'}{1-\eta'}\right)^m}{(m+1)m} - \frac{(1+\xi)^m I_{1\,m}}{(m+1)(1+\varepsilon^2)^{1/2}}. \quad .. \quad .. \quad .. \quad \text{(II.19)}$$

We can now use the identity (for $\eta' < 0{\cdot}5$)

$$\sum_1^\infty \left[(-1)^{m+1}\left(\frac{\eta'}{1-\eta'}\right)^m \frac{1}{(m+1)m}\right] = -\frac{1}{\eta'}\ln(1-\eta') - 1, \quad .. \quad \text{(II.20)}$$

[which can be easily verified by expanding the right-hand side in powers of $\eta'/(1-\eta')$], and, therefore, *finally :*

$$I_1 = \frac{1}{(1+\varepsilon^2)^{1/2}}\left[I_{1\,0}\,\xi - I_{1\,-1}\ln(1-\eta')\right] + (1+\xi)\left[2 + \frac{1}{\eta'}\ln(1-\eta') - \sum_1^\infty T_{1\,m}\right]. \quad \text{(II.21)}$$

A recurrence formula for $T_{1,m}$ has been obtained from that given by Edwards[7] and reproduced in (I.22). This formula, together with (II.19), gives the following recurrence formula for $T_{1\,m}$:

$$T_{1\,m} = \frac{\varepsilon^2}{1+\varepsilon^2}\left[\frac{1+m\xi+(m-1)^2\xi^2}{(m+1)m\,(m-1)(m-2)}\right.$$
$$+ (-1)^m(1+\xi)\frac{\eta'^{m-2}}{(1-\eta')^{m-1}}\,\frac{\eta'[m^2-3m+1-(m-1)^2\xi]+(m-1)^2(1+\xi)}{(m+1)m(m-1)(m-2)}$$
$$\left. - \frac{(m-1)^2}{(m+1)m}(1+\xi)^2\,T_{1,\,m-2} + \frac{2m-1}{m+1}(1+\xi)\,T_{1,\,m-1}\right]$$
$$+ \frac{1}{(m+1)m(1+\varepsilon^2)}\left[1-\sigma_{1\,1} + (-1)^m\frac{\eta'^{m-1}}{(1-\eta')^m}\left\{\eta'(1+\varepsilon^2)-\sigma_{1\,0}\right\}\right]. \quad \text{(II.22)}$$

The above formula gives values of $T_{1\,m}$ for $m > 2$. $T_{1\,1}$, $T_{1\,2}$ are found from (II.13), (II.14) and (II.19). They are:

$$T_{1\,1} = \frac{1}{2}\left[\frac{(1-2\eta')(1+\varepsilon^2)-(1-\eta')\sigma_{1\,1}+\sigma_{1\,0}}{(1-\eta')(1+\varepsilon^2)} - \frac{\varepsilon^2(1+\xi)}{1+\varepsilon^2}\,\frac{I_{1\,0}}{(1+\varepsilon^2)^{1/2}}\right], \quad .. \quad \text{(II.23)}$$

$$T_{1\,2} = \frac{1}{6}\left[\frac{\{(1-\eta')^2+\eta'^2\}(1+\varepsilon^2)^2-(1-\eta')^2(1+4\varepsilon^2+3\varepsilon^2\xi)\sigma_{1\,1}}{(1-\eta')^2(1+\varepsilon^2)^2}\right.$$
$$- \frac{\{\eta'(1+4\varepsilon^2)-3\varepsilon^2-3\varepsilon^2\xi(1-\eta')\}\sigma_{1\,0}}{(1-\eta')^2(1+\varepsilon^2)^2}$$
$$\left. + \frac{\varepsilon^2(1-2\varepsilon^2)(1+\xi)^2}{(1+\varepsilon^2)^2}\,\frac{I_{1\,0}}{(1+\varepsilon^2)^{1/2}}\right]. \quad .. \quad .. \quad .. \quad .. \quad .. \quad \text{(II.24)}$$

The above formulae give now all that is needed for computing I_1 for the inner part of the semi-span in any particular case.

For the *outer part of the semi-span* ($0{\cdot}5 \leqslant \eta' \leqslant 1$), the integral (II.4) requires a special treatment. Except for the elementary term $I_{1\,-1}$, the range of integration will be subdivided into three parts, *viz.*:

$$\left.\begin{array}{r} 0 < \mu < \mu_1 \\ -\mu_1 < \mu < 0 \\ \mu_0 < \mu < -\mu_1 \end{array}\right| \begin{array}{c} \text{corres-} \\ \text{ponding} \\ \text{respec-} \\ \text{tively} \\ \text{to} \end{array} \left|\begin{array}{r} 0 < \mu(1+\xi) < 1 \\ -1 < \mu(1+\xi) < 0 \\ -\eta'/1-\eta' < \mu(1+\xi) < -1 \end{array}\right| \begin{array}{c} \text{or} \\ \text{to} \end{array} \left|\begin{array}{r} \eta' < \bar{\eta} < 1 \\ 2\eta' - 1 < \bar{\eta} < \eta' \\ 0 < \bar{\eta} < 2\eta' - 1 \end{array}\right.$$

and, in the last one of them, the integrand will be split into two additive terms, so that, finally, I_1 will be represented by a *sum of five terms*, thus:

$$(1+\varepsilon^2)^{1/2} I_1 = I_{1h} + I_{1j} + I_{1k} - I_{1p} - I_{1\,-1} \ln(1-\eta'), \quad \ldots\ldots\ldots\ldots \text{(II.25)}$$

where

$$I_{1h} = -\int_{\mu_0}^{\mu_1} \left\{ 1 + \frac{1}{\mu} \ln[1-\mu(1+\xi)] \right\} \frac{d\mu}{R_1}, \quad \ldots\ldots\ldots\ldots \text{(II.26)}$$

$$I_{1j} = -\int_{-\mu_1}^{\mu_0} \left\{ 1 + \frac{1}{\mu} \ln[1-\mu(1+\xi)] \right\} \frac{d\mu}{R_1}, \quad \ldots\ldots\ldots\ldots \text{(II.27)}$$

$$I_{1k} = -\int_{\mu_0}^{-\mu_1} \frac{d\mu}{R_1} = -\ln \frac{\eta' + \varepsilon^2 + \varepsilon^2\xi(1-\eta') + \sigma_{1\,0}(1+\varepsilon^2)^{1/2}}{(1-\eta')\{1+2\varepsilon^2+\varepsilon^2\xi+\sigma_{1\,2}(1+\varepsilon^2)^{1/2}\}}, \quad \ldots\ldots \text{(II.28)}$$

$$I_{1p} = \int_{\mu_0}^{-\mu_1} \frac{\ln[1-\mu(1+\xi)]}{\mu R_1} d\mu. \quad \ldots\ldots\ldots\ldots \text{(II.29)}$$

Here μ and R_1 are still defined by (II.3) and (II.5), $\sigma_{1\,0}$ is given by (II.15), while $\sigma_{1\,2}$ is a new factor making its appearance in R_1 when substituting the limit $\mu = -\mu_1$:

$$\sigma_{1\,2}{}^2 = 1 + \varepsilon^2(\xi+2)^2. \quad \ldots\ldots\ldots\ldots \text{(II.30)}$$

This seemingly awkward subdivision leads to tractable integrals, each of which must be treated in an appropriate way.

The logarithms occurring in I_{1k}, I_{1j} may be expanded in power series just as, previously, for I_1 in the inner range; we then obtain for I_{1k}:

$$I_{1k} = I_{1k0}\,\xi + (1+\xi)\left(1 - \sum_1^\infty T_{1km}\right), \quad \ldots\ldots\ldots\ldots \text{(II.31)}$$

where

$$I_{1k0} = \ln \frac{1-\varepsilon^2\xi+\sigma_{1\,1}(1+\varepsilon^2)^{1/2}}{(1+\xi)\{-\varepsilon^2+\varepsilon(1+\varepsilon^2)^{1/2}\}}, \quad \ldots\ldots\ldots\ldots \text{(II.32)}$$

$$T_{1km} = \frac{1}{(m+1)m} - \frac{(1+\xi)^m}{m+1} I_{1km}, \quad \ldots\ldots\ldots\ldots \text{(II.33)}$$

$$T_{1k1} = \frac{1}{2}\left(1 - \frac{\sigma_{1\,1} - \varepsilon(1+\xi)}{(1+\varepsilon^2)^{1/2}} - \frac{\varepsilon^2(1+\xi)}{1+\varepsilon^2} I_{1k0}\right), \quad \ldots\ldots\ldots\ldots \text{(II.34)}$$

$$T_{1k2} = \frac{1}{6}\left(1 - \frac{(1+4\varepsilon^2+3\varepsilon^2\xi)\sigma_{1\,1} - 3\varepsilon^3(1+\xi)^2}{(1+\varepsilon^2)^{3/2}} + \frac{\varepsilon^2(1-2\varepsilon^2)(1+\xi)^2}{(1+\varepsilon^2)^2} I_{1k0}\right); \quad \ldots\ldots\ldots\ldots \text{(II.35)}$$

the recurrence formula for $T_{1\,h\,m}$ being:

$$T_{1\,h\,m} = \frac{\varepsilon^2}{1+\varepsilon^2}\Big(\frac{1+m\xi+(m-1)^2\xi^2}{(m+1)m(m-1)(m-2)} - \frac{(m-1)^2(1+\xi)^2}{(m+1)m}\,T_{1\,h\,m-2} + \frac{(2m-1)(1+\xi)}{m+1}\,T_{1\,h\,m-1}\Big) + \frac{1}{(m+1)m(1+\varepsilon^2)}\Big(1-\sigma_{1\,1}(1+\varepsilon^2)^{1/2}\Big). \quad \text{(II.36)}$$

Similarly for $I_{1\,j}$:

$$I_{1\,j} = I_{1\,j\,0}\,\xi - (1+\xi)\Big(2\ln 2 - 1 - \sum_1^\infty T_{1\,j\,m}\Big), \quad \text{(II.37)}$$

where

$$I_{1\,j\,0} = \ln\frac{1+2\varepsilon^2+\varepsilon^2\xi+\sigma_{1\,2}(1+\varepsilon^2)^{1/2}}{(1+\xi)\{\varepsilon^2+\varepsilon(1+\varepsilon^2)^{1/2}\}}, \quad \text{(II.38)}$$

$$T_{1\,j\,m} = (-1)^{m+1}\Big(\frac{1}{(m+1)m} - \frac{(1+\xi)^m}{m+1}\,I_{1\,j\,m}\Big), \quad \text{(II.39)}$$

$$T_{1\,j\,1} = \frac{1}{2}\Big(1 - \frac{\sigma_{1\,2}-\varepsilon(1+\xi)}{(1+\varepsilon^2)^{1/2}} + \frac{\varepsilon^2(1+\xi)}{1+\varepsilon^2}\,I_{1\,j\,0}\Big), \quad \text{(II.40)}$$

$$T_{1\,j\,2} = -\frac{1}{6}\Big(1 - \frac{(1-2\varepsilon^2-3\varepsilon^2\xi)\sigma_{1\,2}+3\varepsilon^3(1+\xi)^2}{(1+\varepsilon^2)^{3/2}} + \frac{\varepsilon^2(1-2\varepsilon^2)(1+\xi)^2}{(1+\varepsilon^2)^2}\,I_{1\,j\,0}\Big), \quad \text{(II.41)}$$

the recurrence formula for $T_{1\,j\,m}$ being:

$$(-1)^{m+1}\,T_{1\,j\,m} = \frac{\varepsilon^2}{1+\varepsilon^2}\Big(\frac{3m^2-7m+3+(4m^2-9m+4)\xi+(m-1)^2\xi^2}{(m+1)m(m-1)(m-2)} + (-1)^m\frac{(m-1)^2(1+\xi)^2}{(m+1)m}\,T_{1\,j\,m-2} + (-1)^{m+1}\frac{(2m-1)(1+\xi)}{m+1}\,T_{1\,j\,m-1}\Big) - \frac{\sigma_{1\,2}}{(m+1)m(1+\varepsilon^2)^{1/2}} + \frac{1}{(m+1)m}. \quad \text{(II.42)}$$

As the integral $I_{1\,k}$ is elementary, *there remains only* $I_{1\,p}$, and here we notice that the previous expansion of the logarithm in a power series is not valid, but instead the inverse square root may be expanded in negative powers of $t = -\mu$, thus:

$$I_{1\,p} = -\int_{\mu_1}^{-\mu_0}\Big(\frac{1}{t^2}+\frac{a_3}{t^3}+\frac{a_4}{t^4}+\ldots\Big)\ln[1+t(1+\xi)]\,d\mu, \quad \text{(II.43)}$$

where

$$a_3 = -\frac{\varepsilon^2}{1+\varepsilon^2}, \qquad a_6 = -\frac{\varepsilon^4(3-24\varepsilon^2+8\varepsilon^4)}{8(1+\varepsilon^2)^4},$$
$$a_4 = -\frac{\varepsilon^2(1-2\varepsilon^2)}{2(1+\varepsilon^2)^2}, \qquad a_7 = -\frac{\varepsilon^6(15-40\varepsilon^2+8\varepsilon^4)}{8(1+\varepsilon^2)^5},$$
$$a_5 = -\frac{\varepsilon^4(3-2\varepsilon^2)}{2(1+\varepsilon^2)^3}, \qquad a_8 = -\frac{\varepsilon^6(5-90\varepsilon^2+120\varepsilon^4-16\varepsilon^6)}{16(1+\varepsilon^2)^6}, \text{ etc.} \quad \text{(II.44)}$$

Particular terms of (II.43) may be integrated by parts:

$$\int \frac{\ln [1 + t(1 + \xi)]}{t^n}\, dt = - \frac{\ln [1 + t(1 + \xi)]}{(n - 1)t^{n-1}} + \frac{1 + \xi}{n - 1} \int \frac{dt}{t^{n-1} [1 + t(1 + \xi)]}, \quad .. \quad \text{(II.45)}$$

and then the second term in (II.45) by resolving into partial fractions, and

$$\int \frac{\ln [1 + t(1 + \xi)]}{t^n}\, dt = - \frac{\ln [1 + t(1 + \xi)]}{(n - 1)t^{n-1}} + \frac{1 + \xi}{n - 1} \Big[- \frac{1}{(n - 2)t^{n-2}} + \frac{1 + \xi}{(n - 3)t^{n-3}}$$

$$- \frac{(1 + \xi)^2}{(n - 4)t^{n-4}} + - \ldots \pm \frac{(1 + \xi)^{n-3}}{t} \pm (1 + \xi)^{n-2} \ln \Big(\frac{t}{1 + t(1 + \xi)} \Big) \Big]. \quad .. \quad .. \quad \text{(II.46)}$$

Substituting the corresponding values of the above in (II.43) we obtain:

$$I_{1p} = - [P_{1p1} + a_3 P_{1p2} + a_4 P_{1p3} + \ldots] \quad .. \quad .. \quad .. \quad .. \quad .. \quad \text{(II.47)}$$

where

$$\left.\begin{aligned}
P_{1p1} &= (1 + \xi) \Big(\frac{1 - \eta'}{\eta'} \ln (1 - \eta') + \ln 4\eta' \Big) \\
P_{1p2} &= (1 + \xi)^2 \Big(\frac{(1 - \eta')^2}{2\eta'^2} \ln (1 - \eta') - \tfrac{1}{2} \ln \eta' + \frac{2\eta' - 1}{2\eta'} \Big) \\
P_{1p3} &= (1 + \xi)^3 \Big(\frac{(1 - \eta')^3}{3\eta'^3} \ln (1 - \eta') + \tfrac{1}{3} \ln 4\eta' - \frac{(2\eta' - 1)^2}{6\eta'^2} \Big) \\
P_{1p4} &= (1 + \xi)^4 \Big(\frac{(1 - \eta')^4}{4\eta'^4} \ln (1 - \eta') - \tfrac{1}{4} \ln \eta' + \frac{(2\eta' - 1)(8\eta'^2 - 5\eta' + 2)}{24\eta'^3} \Big) \\
P_{1p5} &= (1 + \xi)^5 \Big(\frac{(1 - \eta')^5}{5\eta'^5} \ln (1 - \eta') + \tfrac{1}{5} \ln 4\eta' - \frac{(2\eta' - 1)^2(8\eta'^2 - 4\eta' + 3)}{60\eta'^4} \Big) \\
P_{1p6} &= (1 + \xi)^6 \Big(\frac{(1 - \eta')^6}{6\eta'^6} \ln (1 - \eta') - \tfrac{1}{6} \ln \eta' \\
&\quad + \frac{(2\eta' - 1)(92\eta'^4 - 104\eta'^3 + 98\eta'^2 - 51\eta' + 12)}{360\eta'^5} \Big) \\
P_{1p7} &= (1 + \xi)^7 \Big(\frac{(1 - \eta')^7}{7\eta'^7} \ln (1 - \eta') + \tfrac{1}{7} \ln 4\eta' \\
&\quad - \frac{(2\eta' - 1)^2(46\eta'^4 - 44\eta'^3 + 57\eta'^2 - 32\eta' + 10)}{420\eta'^6} \Big)
\end{aligned}\right\} \quad \text{(II.48)}$$

The above formulae give now all that is needed for computing I_1 for the outer part of the semi-span in any particular case.

The corresponding formulae for I_2 are found from those for I_1 by replacing ξ by $(- \xi)$.

(B) *Contribution of the Left-hand Half-wing.*—Let us consider

$$I_3 = - \int_0^1 \Big[1 + (1 + \eta') \Big(1 + \xi \frac{1 - \eta'}{1 + \eta'} \Big) \frac{\ln (1 - \bar{\eta})}{\bar{\eta} + \eta'} \Big] \frac{d\bar{\eta}}{\varrho_3}. \quad .. \quad .. \quad .. \quad \text{(II.49)}$$

I_3 has been obtained from I_1 by writing $(- \eta')$ for η' and $\Big(\xi \frac{1 - \eta'}{1 + \eta'} \Big)$ for ξ (*see* (3.17)). This rule, however, cannot be applied throughout the subsequent transformation which, fortunately, becomes much simpler than that of I_1.

Introducing a new auxiliary variable

$$\tau = \frac{\bar{\eta} + \eta'}{(1+\eta')\left(1 + \xi\dfrac{1-\eta'}{1+\eta'}\right)}, \quad .. \quad .. \quad .. \quad .. \quad .. \quad .. \quad .. \quad \text{(II.50)}$$

I_3 may be written:

$$I_3 = -\int_{\tau_0}^{\tau_1}\left\{1 + \frac{1}{\tau}\ln(1+\eta') + \frac{1}{\tau}\ln\left[1 - \tau\left(1 + \xi\frac{1-\eta'}{1+\eta'}\right)\right]\right\}\frac{d\tau}{R_3(1+\varepsilon^2)^{1/2}}, \quad \text{(II.51)}$$

where

$$R_3^2 = \tau^2 - 2\frac{\varepsilon^2}{1+\varepsilon^2}\tau + \frac{\varepsilon^2}{1+\varepsilon^2}, \quad .. \quad .. \quad .. \quad .. \quad .. \quad .. \quad \text{(II.52)}$$

this again being much simpler than ϱ_3^2, and the lower and upper limits of integration become:

$$\left.\begin{aligned}\tau_0 &= \frac{\eta'}{(1+\eta')\left(1 + \xi\dfrac{1-\eta'}{1+\eta'}\right)},\\ \tau_1 &= \frac{1}{1 + \xi\dfrac{1-\eta'}{1+\eta'}}.\end{aligned}\right| \quad .. \quad .. \quad .. \quad .. \quad .. \quad .. \quad \text{(II.53)}$$

For I_3, also, we may expand the logarithm in a power series, valid throughout the range of integration. I_3 then becomes:

$$I_3 = \frac{1}{(1+\varepsilon^2)^{1/2}}\left[I_{3\,0}\,\xi\frac{1-\eta'}{1+\eta'} - I_{3\,-1}\ln(1+\eta') + \sum_{m=1}^{\infty}\frac{\left(1 + \xi\dfrac{1-\eta'}{1+\eta'}\right)^{m+1}}{m+1}I_{3\,m}\right], \quad .. \quad \text{(II.54)}$$

where the particular terms (for m from -1 to $+\infty$) are defined by:

$$I_{3\,m} = \int_{\tau_0}^{\tau_1}\frac{\tau^m}{R_3}\,d\tau, \quad .. \quad .. \quad .. \quad .. \quad .. \quad .. \quad .. \quad .. \quad \text{(II.55)}$$

and the first of them becomes:

$$I_{3\,-1} = \int_{\tau_0}^{\tau_1}\frac{d\tau}{\tau R_3} = -\frac{(1+\varepsilon^2)^{1/2}}{\varepsilon}\left|\ln\frac{\varepsilon - \varepsilon\tau + R_3(1+\varepsilon^2)^{1/2}}{|\tau|}\right|_{\tau_0}^{\tau_1}, \quad .. \quad .. \quad \text{(II.56)}$$

or

$$I_{3\,-1} = \frac{(1+\varepsilon^2)^{1/2}}{\varepsilon}\ln\left[\frac{\varepsilon + \varepsilon\xi(1-\eta') + \sigma_{3\,0}}{\eta'\left(\varepsilon\xi\dfrac{1-\eta'}{1+\eta'} + \sigma_{3\,1}\right)}\right]; \quad .. \quad .. \quad .. \quad .. \quad .. \quad \text{(II.57)}$$

$\sigma_{3\,0}^2$, $\sigma_{3\,1}^2$ are the following factors appearing in the expressions for R_3^2 obtained after substituting the lower and upper limits of integration, respectively:

$$\left.\begin{aligned}\sigma_{3\,0}^2 &= \eta'^2 + \varepsilon^2[1 + \xi(1-\eta')]^2 = \sigma_{1\,0}^2,\\ \sigma_{3\,1}^2 &= 1 + \varepsilon^2\xi^2\left(\frac{1-\eta'}{1+\eta'}\right)^2\end{aligned}\right| \quad .. \quad .. \quad .. \quad .. \quad .. \quad \text{(II.58)}$$

It will be seen by comparing (II.57) with (II.11) that the general rule for obtaining the contribution of the left-hand half-wing from that of the right (as obtained previously for $\eta' < 0{\cdot}5$) does not apply for this case. This is due to the modulus of the variable (μ or τ) in the denominator of the indefinite integral (*see* II.10 and II.56) which results in the factor η' occurring with a positive sign in the denominators of both $I_{1\,-1}$ and $I_{3\,-1}$.

The next three integrals of the type (II.55) become:

$$I_{3\,0} = \ln \frac{(1+\eta')\left(1 - \varepsilon^2\xi\dfrac{1-\eta'}{1+\eta'} + \sigma_{3\,1}(1+\varepsilon^2)^{1/2}\right)}{\eta' - \varepsilon^2 - \varepsilon^2\xi(1-\eta') + \sigma_{3\,0}(1+\varepsilon^2)^{1/2}}, \quad .. \quad .. \quad .. \quad \text{(II.59)}$$

$$I_{3\,1} = \frac{(1+\eta')\sigma_{3\,1} - \sigma_{3\,0}}{(1+\eta')\left(1+\xi\dfrac{1-\eta'}{1+\eta'}\right)(1+\varepsilon^2)^{1/2}} + \frac{\varepsilon^2}{1+\varepsilon^2} I_{3\,0}, \quad .. \quad .. \quad .. \quad \text{(II.60)}$$

$$I_{3\,2} = \frac{(1+\eta')^2\left(1+4\varepsilon^2+3\varepsilon^2\xi\dfrac{1-\eta'}{1+\eta'}\right)\sigma_{3\,1} - [\eta'(1+4\varepsilon^2)+3\varepsilon^2+3\varepsilon^2\xi(1-\eta')]\sigma_{3\,0}}{2(1+\eta')^2\left(1+\xi\dfrac{1-\eta'}{1+\eta'}\right)^2(1+\varepsilon^2)^{3/2}}$$
$$- \frac{\varepsilon^2(1-2\varepsilon^2)}{2(1+\varepsilon^2)^2} I_{3\,0}. \quad .. \quad .. \quad .. \quad .. \quad .. \quad .. \quad .. \quad \text{(II.61)}$$

We introduce, again, another series which is composed of the terms:

$$\left.\begin{aligned}(I_{3\,1})_{\varepsilon=0} &= \frac{1-\dfrac{\eta'}{1+\eta'}}{1+\xi\dfrac{1-\eta'}{1+\eta'}} \\ (I_{3\,2})_{\varepsilon=0} &= \frac{1-\left(\dfrac{\eta'}{1+\eta'}\right)^2}{2\left(1+\xi\dfrac{1-\eta'}{1+\eta'}\right)^2}, \text{ etc.:}\end{aligned}\right| \quad .. \quad .. \quad .. \quad .. \quad .. \quad .. \quad \text{(II.62)}$$

(the rule for converting I_1 into I_3 again does not apply), and I_3 may be written

$$I_3 = \frac{1}{(1+\varepsilon^2)^{1/2}}\left(I_{3\,0}\,\xi\frac{1-\eta'}{1+\eta'} - I_{3\,-1}\ln(1+\eta')\right)$$
$$+\left(1+\xi\frac{1-\eta'}{1+\eta'}\right)\left[\sum_1^\infty \frac{1}{(m+1)m} - \sum_1^\infty \frac{1}{(m+1)m}\left(\frac{\eta'}{1+\eta'}\right)^m - \sum_1^\infty T_{3\,m}\right], \quad .. \quad \text{(II.63)}$$

where

$$T_{3\,m} = \frac{1-\left(\dfrac{\eta'}{1+\eta'}\right)^m}{(m+1)m} - \frac{\left(1+\xi\dfrac{1-\eta'}{1+\eta'}\right)^m}{m+1}\frac{I_{3\,m}}{(1+\varepsilon^2)^{1/2}} \quad .. \quad .. \quad .. \quad \text{(II.64)}$$

We can now introduce the following identity (valid for any positive η'), analogous to (II.20):

$$\sum_1^\infty \left[\frac{1}{(m+1)m}\left(\frac{\eta'}{1+\eta'}\right)^m\right] = 1 - \frac{1}{\eta'}\ln(1+\eta'), \quad .. \quad .. \quad .. \quad \text{(II.65)}$$

and therefore, *finally*:

$$I_3 = \frac{1}{(1+\varepsilon^2)^{1/2}}\left[I_{3\,0}\,\xi\frac{1-\eta'}{1+\eta'} - I_{3\,-1}\ln(1+\eta')\right]$$
$$+\left(1+\xi\frac{1-\eta'}{1+\eta'}\right)\left[\frac{1}{\eta'}\ln(1+\eta') - \sum_1^\infty T_{3\,m}\right]. \quad .. \quad .. \quad .. \quad \text{(II.66)}$$

The first two terms of $T_{3\,m}$ are found directly from (II.60), (II.61) and (II.64):

$$T_{3\,1} = \frac{1}{2}\left[\frac{1+\varepsilon^2-(1+\eta')\sigma_{3\,1}+\sigma_{3\,0}}{(1+\varepsilon^2)(1+\eta')} - \frac{\varepsilon^2\left(1+\xi\dfrac{1-\eta'}{1+\eta'}\right)}{1+\varepsilon^2}\frac{I_{3\,0}}{(1+\varepsilon^2)^{1/2}}\right], \quad .. \quad \text{(II.67)}$$

$$\begin{aligned} T_{3\,2} = \frac{1}{6}\Bigg[& \frac{(1+2\eta')(1+\varepsilon^2)^2-(1+\eta')^2\left(1+4\varepsilon^2+3\varepsilon^2\xi\dfrac{1-\eta'}{1+\eta'}\right)\sigma_{3\,1}}{(1+\eta')^2(1+\varepsilon^2)^2} \\ & + \frac{\{\eta'(1+4\varepsilon^2)+3\varepsilon^2+3\varepsilon^2\xi(1-\eta'\}\sigma_{3\,0}}{(1+\eta')^2(1+\varepsilon^2)^2} \\ & + \frac{\varepsilon^2(1-2\varepsilon^2)\left(1+\xi\dfrac{1-\eta'}{1+\eta'}\right)^2}{(1+\varepsilon^2)^2}\frac{I_{3\,0}}{(1+\varepsilon^2)^{1/2}}\Bigg], \quad .. \quad .. \quad .. \quad .. \quad \text{(II.68)} \end{aligned}$$

and the recurrence formula for subsequent ones is found as before by using the formula given by Edwards[7] and reproduced in (I.22):

$$\begin{aligned} T_{3\,m} = \frac{\varepsilon^2}{1+\varepsilon^2}\Bigg[& \frac{1+m\xi\dfrac{1-\eta'}{1+\eta'}+(m-1)^2\xi^2\left(\dfrac{1-\eta'}{1+\eta'}\right)^2}{(m+1)m(m-1)(m-2)} + \frac{\left(1+\xi\dfrac{1-\eta'}{1+\eta'}\right)\eta'^{m-2}}{(1+\eta')^{m-1}} \\ & \times \frac{\eta'\left[m^2-3m+1-(m-1)^2\xi\dfrac{1-\eta'}{1+\eta'}\right]-(m-1)^2\left(1+\xi\dfrac{1-\eta'}{1+\eta'}\right)}{(m+1)m(m-1)(m-2)} \\ & - \frac{(m-1)^2\left(1+\xi\dfrac{1-\eta'}{1+\eta'}\right)^2}{(m+1)m}T_{3,\,m-2} + \frac{(2m-1)\left(1+\xi\dfrac{1-\eta'}{1+\eta'}\right)}{m+1}T_{3,\,m-1}\Bigg] \\ & + \frac{1}{(m+1)m(1+\varepsilon^2)}\left[1-\sigma_{3\,1}-\frac{\eta'^{m-1}}{(1+\eta')^m}\left\{\eta'(1+\varepsilon^2)-\sigma_{3\,0}\right\}\right]. \quad .. \quad \text{(II.69)} \end{aligned}$$

The above formulae give now all that is needed for computing I_3 in any particular case.

The corresponding formulae for I_4 are found from those for I_3 by replacing ξ by $(-\xi)$.

The formulae for the central section, mid-chord line and wing centre may now be found by substituting $\eta' = 0$ and/or $\xi = 0$ in these final formulae, without any difficulties arising. The expansions for I_1 and I_2 break down at the sharp tip, but that was to be expected because these integrals present a logarithmic singularity for $\eta' = 1$, as seen directly from (3.17).

APPENDIX III (To Section 4)

Velocity Distribution over the Entire Surface of a Cropped Rhombus Wing with Biconvex Parabolic Profile and Spanwise Constant Thickness Ratio

The velocity distribution over the surface of the right-hand half of a cropped-rhombus wing, due to the right or left cut-off tip triangles, respectively, is given by (4.2), *viz.* :

$$\left.\begin{aligned} -\pi\hat{v}_{x\,r}/U\vartheta &= \Omega + \bar{I}_1 + \bar{I}_2\,, \\ -\pi\hat{v}_{x\,l}/U\vartheta &= \Lambda + \bar{I}_3 + \bar{I}_4\,, \end{aligned}\right\} \quad .. \quad .. \quad .. \quad .. \quad .. \quad .. \quad .. \quad .. \quad \text{(III.1)}$$

where Ω, Λ, $\bar{I}_1$, $\bar{I}_2$, $\bar{I}_3$, $\bar{I}_4$, are defined in (4.3) and (4.4). The above values must be subtracted from those found in Appendix II for the full-rhombus wing.

As for the full-rhombus wing, we shall consider here the general case of arbitrary values of η' and ξ within the wing area, but, as before, the formulae will still apply for the special cases of central section, mid-chord line and wing centre, and will become simpler for them, although not so markedly as for the full-rhombus wing.

(A) *Contribution of the Right-hand Tip Triangle.*—Let us consider

$$\bar{I}_1 = -\int_{1-\psi}^{1}\left(1 + (1-\eta')(1+\xi)\frac{\ln(1-\bar{\eta})}{\bar{\eta}-\eta'}\right)\frac{d\bar{\eta}}{\varrho_1}\,; \quad .. \quad .. \quad .. \quad .. \quad \text{(III.2)}$$

substituting the same auxiliary variable as before (*see* II.3):

$$\mu = \frac{\bar{\eta}-\eta'}{(1-\eta')(1+\xi)}\,, \quad .. \quad .. \quad .. \quad .. \quad .. \quad .. \quad .. \quad \text{(III.3)}$$

and expanding the logarithm as for the complete rhombus, we obtain

$$\bar{I}_1 = \frac{1}{(1+\varepsilon^2)^{1/2}}\left[\xi\bar{I}_{1\,0} - \bar{I}_{1\,-1}\ln(1-\eta') + \sum_{m=1}^{\infty}\frac{(1+\xi)^{m+1}}{m+1}\bar{I}_{1\,m}\right], \quad .. \quad .. \quad \text{(III.4)}$$

where

$$\bar{I}_{1\,m} = \int_{\mu_{1-\psi}}^{\mu_1}\frac{\mu^m}{R_1}\,d\mu \quad .. \quad .. \quad .. \quad .. \quad .. \quad .. \quad .. \quad .. \quad .. \quad \text{(III.5)}$$

and

$$R_1^2 = \mu^2 - 2\mu\frac{\varepsilon^2}{1+\varepsilon^2} + \frac{\varepsilon^2}{1+\varepsilon^2}\,, \quad .. \quad .. \quad .. \quad .. \quad .. \quad .. \quad \text{(III.6)}$$

$$\left.\begin{aligned} \mu_{1-\psi} &= \frac{1-\psi-\eta'}{(1-\eta')(1+\xi)} \\ \mu_1 &= \frac{1}{1+\xi}\,. \end{aligned}\right\} \quad .. \quad .. \quad .. \quad .. \quad .. \quad .. \quad .. \quad .. \quad \text{(III.7)}$$

Hence

$$\bar{I}_{1\,-1} = \int_{\mu_{1-\psi}}^{\mu_1}\frac{d\mu}{\mu R_1} = \frac{(1+\varepsilon^2)^{1/2}}{\varepsilon}\ln\left(\frac{\varepsilon\xi(1-\eta') + \varepsilon\psi + \hat{\sigma}_{1,1-\psi}}{(1-\eta'-\psi)(\varepsilon\xi + \hat{\sigma}_{1\,1})}\right), \quad .. \quad .. \quad \text{(III.8)}$$

$$\bar{I}_{1\,0} = \ln\frac{(1-\eta')\{1-\varepsilon^2\xi + \sigma_{1\,1}(1+\varepsilon^2)^{1/2}\}}{1-\eta'-\psi(1+\varepsilon^2) - \varepsilon^2\xi(1-\eta') + \hat{\sigma}_{1,1-\psi}(1+\varepsilon^2)^{1/2}}\,, \quad .. \quad .. \quad \text{(III.9)}$$

$$\bar{I}_{1\,1} = \frac{(1-\eta')\hat{\sigma}_{1,1} - \hat{\sigma}_{1,1-\psi}}{(1+\xi)(1-\eta')\,(1+\varepsilon^2)^{1/2}} + \frac{\varepsilon^2}{1+\varepsilon^2}\bar{I}_{1\,0}\,, \quad .. \quad .. \quad .. \quad .. \quad \text{(III.10)}$$

$$\bar{I}_{1\,2} = \frac{(1-\eta')^2(1+4\varepsilon^2+3\varepsilon^2\xi)\hat{\sigma}_{1\,1} - [1-\eta'-\psi-\varepsilon^2\psi+\varepsilon^2(1-\eta')(4+3\xi)]\hat{\sigma}_{1;1-\psi}}{2(1+\varepsilon)^2(1-\eta')^2(1+\varepsilon^2)^{3/2}}$$

$$- \frac{\varepsilon^2(1-2\varepsilon^2)}{2(1+\varepsilon^2)^2}\,\bar{I}_{1\,0}\,. \qquad .. \quad .. \quad .. \quad .. \quad .. \quad \text{(III.11)}$$

$\hat{\sigma}_{1,1-\psi}{}^2$, $\hat{\sigma}_{1\,1}{}^2$ are the following factors appearing in the expressions for $R_1{}^2$ obtained after substituting the lower and upper limits of integration, respectively:

$$\left.\begin{aligned} \hat{\sigma}_{1,1-\psi}{}^2 &= (1-\eta'-\psi)^2 + \varepsilon^2\{\psi+\xi(1-\eta')\}^2\,, \\ \hat{\sigma}_{1\,1}{}^2 &= \sigma_{1\,1}{}^2 = 1+\varepsilon^2\xi^2\,. \end{aligned}\right\} \quad .. \quad .. \quad .. \quad .. \quad .. \quad \text{(III.12)}$$

The expansion of the logarithm in a power series, used here, is valid throughout the range of integration.

We now consider a series obtained from that of (III.4) by letting $\varepsilon \to 0$ in a similar way to that for the full rhombus:

$$\left.\begin{aligned} (\bar{I}_{1\,1})_{\varepsilon\to 0} &= \frac{1}{1+\xi}\left(1-\frac{1-\eta'-\psi}{1-\eta'}\right), \\ (\bar{I}_{1\,2})_{\varepsilon\to 0} &= \frac{1}{2(1+\xi)^2}\left[1-\left(\frac{1-\eta'-\psi}{1-\eta'}\right)^2\right], \text{ etc.} \end{aligned}\right\} \quad .. \quad .. \quad .. \quad .. \quad \text{(III.13)}$$

$\bar{I}_1$ may then be written:

$$\bar{I}_1 = \frac{1}{(1+\varepsilon^2)^{1/2}}\left[\bar{I}_{1\,0}\xi - \bar{I}_{1\,-1}\ln(1-\eta')\right] + \sum_{m=1}^{\infty}\left[\frac{(1+\xi)^{m+1}}{(m+1)m}\left\{\frac{1-\left(\frac{1-\eta'-\psi}{1-\eta'}\right)^m}{(1+\xi)^m}\right.\right.$$

$$\left.\left. - \frac{1-\left(\frac{1-\eta'-\psi}{1-\eta'}\right)^m}{(1+\xi)^m} + m\frac{\bar{I}_{1\,m}}{(1+\varepsilon^2)^{1/2}}\right\}\right], \qquad .. \quad .. \quad .. \quad .. \quad \text{(III.14)}$$

or

$$\bar{I}_1 = \frac{1}{(1+\varepsilon^2)^{1/2}}\left[\bar{I}_{1\,0}\xi - \bar{I}_{1\,-1}\ln(1-\eta')\right] + (1+\xi)\left[\sum_1^{\infty}\frac{1}{(m+1)m}\right.$$

$$\left. - \sum_1^{\infty}\frac{1}{(m+1)m}\left(\frac{1-\eta'-\psi}{1-\eta'}\right)^m - \sum_1^{\infty}\hat{T}_{1\,m}\right], \qquad .. \quad .. \quad .. \quad \text{(III.15)}$$

where

$$\hat{T}_{1\,m} = \frac{1-\left(\frac{1-\eta'-\psi}{1-\eta'}\right)^m}{(m+1)m} - \frac{(1+\xi)^m\,\bar{I}_{1\,m}}{(m+1)(1+\varepsilon^2)^{1/2}}\,. \qquad .. \quad .. \quad .. \quad .. \quad \text{(III.16)}$$

We can now use the obvious relationship (analogous to II.20)

$$\sum_1^{\infty}\frac{1}{(m+1)m}\left(\frac{1-\eta'-\psi}{1-\eta'}\right)^m = \frac{\psi}{1-\eta'-\psi}\ln\left(\frac{\psi}{1-\eta'}\right)+1\,, \quad .. \quad \text{(III.17)}$$

and then *finally*:

$$\bar{I}_1 = \frac{1}{(1+\varepsilon^2)^{1/2}}\left[\bar{I}_{1\,0}\xi - \bar{I}_{1\,-1}\ln(1-\eta')\right] - (1+\xi)\left[\frac{\psi}{1-\eta'-\psi}\ln\frac{\psi}{1-\eta'} + \sum_1^{\infty}\hat{T}_{1\,m}\right].$$

$$.. \quad .. \quad .. \quad \text{(III.18)}$$

Using the recurrence formula given by Edwards[7], reproduced in (I.22), and the relationship (III.16), we get for $\hat{T}_{1\,m}$:

$$\hat{T}_{1\,m} = \frac{\varepsilon^2}{1+\varepsilon^2}\left[\frac{1+m\xi+(m-1)\xi^2}{(m+1)m(m-1)(m-2)} + \frac{(1+\xi)(1-\eta'-\psi)^{m-2}}{(1-\eta')^{m-1}}\right.$$
$$\times \frac{(1-\eta')[m^2-3m+1-(m-1)^2\xi]-\psi(2m^2-5m+2)}{(m+1)m(m-1)(m-2)}$$
$$\left. - \frac{(m-1)^2(1+\xi)^2}{(m+1)m}\hat{T}_{1\,m-2} + \frac{(2m-1)(1+\xi)}{m+1}\hat{T}_{1\,m-1}\right]$$
$$+ \frac{1}{(m+1)m(1+\varepsilon^2)}\left[1-\hat{\sigma}_{1\,1} - \frac{(1-\eta'-\psi)^{m-1}}{(1-\eta')^m}[(1-\eta'-\psi)(1+\varepsilon^2)-\hat{\sigma}_{1,1-\psi}]\right]$$
.. .. .. (III.19)

This formula is applicable for all values of m greater than 2. $\hat{T}_{1\,1}$, $\hat{T}_{1\,2}$ are found from (III.10), (III.11) and (III.16):

$$\hat{T}_{1\,1} = \frac{1}{2}\left[\frac{[(1-\eta')-(1-\eta'-\psi)](1+\varepsilon^2)-(1-\eta')\hat{\sigma}_{1\,1}+\hat{\sigma}_{1,1-\psi}}{(1-\eta')(1+\varepsilon^2)}\right.$$
$$\left. - \frac{\varepsilon^2}{1+\varepsilon^2}(1+\xi)\frac{\bar{I}_{1\,0}}{(1+\varepsilon^2)^{1/2}}\right], \quad .. \quad .. \quad .. \quad .. \quad .. \quad .. \quad \text{(III.20)}$$

$$\hat{T}_{1\,2} = \frac{1}{6}\left[\frac{[(1-\eta')^2-(1-\eta'-\psi)^2](1+\varepsilon^2)^2-(1-\eta')^2(1+4\varepsilon^2+3\varepsilon^2\xi)\hat{\sigma}_{1\,1}}{(1-\eta')^2(1+\varepsilon^2)^2}\right.$$
$$+ \frac{[1-\eta'-\psi-\varepsilon^2\psi+4\varepsilon^2(1-\eta')+3\varepsilon^2\xi(1-\eta')]\hat{\sigma}_{1,1-\psi}}{(1-\eta')^2(1+\varepsilon^2)^2}$$
$$\left. + \frac{\varepsilon^2(1-2\varepsilon^2)(1+\xi)^2}{(1+\varepsilon^2)^2}\frac{\bar{I}_{1\,0}}{(1+\varepsilon^2)^{1/2}}\right]. \quad .. \quad .. \quad .. \quad .. \quad .. \quad \text{(III.21)}$$

The above formulae give now all that is needed for computing $\bar{I}_1$ in any particular case.

The corresponding formulae for $\bar{I}_2$ are found by replacing ξ by $(-\xi)$ in those for $\bar{I}_1$.

(B) *Contribution of the Left-hand Tip Triangle.*—In this case (of a cropped-rhombus wing), the rule for obtaining the formulae for the left-hand half-wing from those for the right-hand half-wing can be applied, *i.e.*, we replace η' by $(-\eta')$ and ξ by $\left(\xi\frac{1-\eta'}{1+\eta'}\right)$. $\bar{I}_3$ then becomes:

$$\bar{I}_3 = \frac{1}{(1+\varepsilon^2)^{1/2}}\left[\bar{I}_{3\,0}\,\xi\frac{1-\eta'}{1+\eta'} - \bar{I}_{3\,-1}\ln(1+\eta')\right]$$
$$- \left(1+\xi\frac{1-\eta'}{1+\eta'}\right)\left[\frac{\psi}{1+\eta'+\psi}\ln\left(\frac{\psi}{1+\eta'}\right)+\sum_1^\infty \hat{T}_{3\,m}\right], \quad .. \quad .. \quad \text{(III.22)}$$

where

$$\bar{I}_{3\,-1} = \frac{(1+\varepsilon^2)^{1/2}}{\varepsilon}\ln\left[\frac{\varepsilon\xi(1-\eta')+\varepsilon\psi+\hat{\sigma}_{3,1-\psi}}{(1+\eta'-\psi)\left(\varepsilon\xi\frac{1-\eta'}{1+\eta'}+\hat{\sigma}_{3\,1}\right)}\right], \quad .. \quad .. \quad \text{(III.23)}$$

$$\bar{I}_{3\,0} = \ln\left[\frac{(1+\eta')\left(1-\varepsilon^2\xi\frac{1-\eta'}{1+\eta'}+\hat{\sigma}_{3\,1}(1+\varepsilon^2)^{1/2}\right)}{1+\eta'-\psi(1+\varepsilon^2)-\varepsilon^2\xi(1-\eta')+\hat{\sigma}_{3,1-\psi}(1+\varepsilon^2)^{1/2}}\right], \quad .. \quad .. \quad \text{(III.24)}$$

$$\hat{T}_{3\,1}=\frac{1}{2}\left[\frac{[(1+\eta')-(1+\eta'-\psi)](1+\varepsilon^2)-(1+\eta')\hat{\sigma}_{3\,1}+\hat{\sigma}_{3,\,1-\psi}}{(1+\eta')(1+\varepsilon^2)}\right.$$
$$\left.-\frac{\varepsilon\left(1+\xi\frac{1-\eta'}{1+\eta'}\right)}{1+\varepsilon^2}\frac{\bar{I}_{3\,0}}{(1+\varepsilon^2)^{1/2}}\right] \quad .. \quad .. \quad .. \quad .. \quad .. \quad .. \quad \text{(III.25)}$$

$$\hat{T}_{3\,2}=\frac{1}{6}\left[\frac{[(1+\eta')^2-(1+\eta'-\psi)^2](1+\varepsilon^2)^2-(1+\eta')^2\left(1+4\varepsilon^2+3\varepsilon^2\xi\frac{1-\eta'}{1+\eta'}\right)\hat{\sigma}_{3\,1}}{(1+\eta')^2(1+\varepsilon^2)^2}\right.$$
$$+\frac{[1+\eta'-\psi-\varepsilon^2\psi+4\varepsilon^2(1+\eta')+3\varepsilon^2\xi(1-\eta')]\sigma_{3,1-\psi}}{(1+\eta')^2(1+\varepsilon^2)^2}$$
$$\left.+\frac{\varepsilon^2(1-2\varepsilon^2)\left(1+\xi\frac{1-\eta'}{1+\eta'}\right)^2}{(1+\varepsilon^2)^2}\frac{\bar{I}_{3\,0}}{(1+\varepsilon^2)^{1/2}}\right] \quad .. \quad .. \quad .. \quad .. \quad \text{(III.26)}$$

The recurrence formula for $\hat{T}_{3\,m}$ is

$$\hat{T}_{3\,m}=\frac{\varepsilon^2}{1+\varepsilon^2}\left[\frac{1+m\xi\frac{1-\eta'}{1+\eta'}+(m-1)^2\xi^2\left(\frac{1-\eta'}{1+\eta'}\right)^2}{(m+1)m(m-1)(m-2)}\right.$$
$$+\frac{\left(1+\xi\frac{1-\eta'}{1+\eta'}\right)(1+\eta'-\psi)^{m-2}}{(1+\eta')^{m-1}}$$
$$\times\frac{(1+\eta')\left[m^2-3m+1-(m-1)^2\xi\frac{1-\eta'}{1+\eta'}\right]-\psi(2m^2-5m+2)}{(m+1)m(m-1)(m-2)}$$
$$\left.-\frac{(m-1)^2\left(1+\xi\frac{1-\eta'}{1+\eta'}\right)^2}{(m+1)m}\hat{T}_{3,m-2}+\frac{(2m-1)\left(1+\xi\frac{1-\eta'}{1+\eta'}\right)}{m+1}\hat{T}_{3,m-1}\right]$$
$$+\frac{1}{(m+1)m(1+\varepsilon^2)}\left[1-\hat{\sigma}_{3\,1}-\frac{(1+\eta'-\psi)^{m-1}}{(1+\eta')^m}\times\left((1+\eta'-\psi)(1+\varepsilon^2)-\hat{\sigma}_{3,1-\psi}\right)\right]\cdot$$
$$.. \quad .. \quad \text{(III.27)}$$

$\hat{\sigma}_{3,1-\psi}{}^2$, $\hat{\sigma}_{3\,1}{}^2$ are the following factors occurring in expressions for $R_3{}^2$ when the lower and upper limits of integration are substituted, respectively:

$$\left.\begin{aligned}\hat{\sigma}_{3,1-\psi}{}^2&=(1+\eta'-\psi)^2+\varepsilon^2[\psi+\xi(1-\eta')]^2,\\ \hat{\sigma}_{3\,1}{}^2&=\sigma_{3\,1}{}^2=1+\varepsilon^2\xi^2\left(\frac{1-\eta'}{1+\eta'}\right)^2.\end{aligned}\right\} \quad .. \quad .. \quad .. \quad .. \quad .. \quad \text{(III.28)}$$

The above formulae are all that is needed for computing $\bar{I}_3$. The corresponding formulae for $\bar{I}_4$ may be found from those for $\bar{I}_3$ by replacing ξ by $(-\xi)$.

The formulae for the central section, mid-chord line and wing centre may now be found by substituting $\eta'=0$ and/or $\xi=0$ in the general formulae for $\bar{I}_1$, $\bar{I}_2$, $\bar{I}_3$, $\bar{I}_4$. These formulae hold good for all values of η' and ξ, even at the tips of the cropped wing; although, in this last case, putting $\eta'=1-\psi$ results in the formulae for $\bar{I}_1$ and $\bar{I}_2$ becoming formally indeterminate. This is easily resolved, however, by finding the limiting values for $\eta'\to 1-\psi$.

TABLE 1

Supervelocities at the Centres of Straight Tapered Wings with Varying Taper Ratio ψ and Coefficient of Convergence ε. Biconvex Parabolic Profile. Illustrated in Figs. 4 and 5

$$-\frac{\pi v_x}{4U\vartheta}$$

ψ	$\varepsilon = 0{\cdot}1$	$\varepsilon = 0{\cdot}2$	$\varepsilon = 0{\cdot}3$	$\varepsilon = 0{\cdot}4$	$\varepsilon = 0{\cdot}5$	$\varepsilon = 0{\cdot}6$	$\varepsilon = 0{\cdot}7$	$\varepsilon = 0{\cdot}8$	$\varepsilon = 0{\cdot}9$	$\varepsilon = 1{\cdot}0$
0	0·958	0·925	0·897	0·872	0·850	0·829	0·811	0·794	0·779	0·764
0·1	0·958	0·925	0·897	0·872	0·850	0·829	0·811	0·794	0·779	0·764
0·2	0·958	0·925	0·897	0·872	0·849	0·829	0·810	0·793	0·777	0·763
0·3	0·958	0·925	0·896	0·871	0·848	0·827	0·808	0·790	0·774	0·758
0·4	0·958	0·924	0·895	0·868	0·844	0·822	0·801	0·782	0·764	0·746
0·5	0·958	0·922	0·891	0·862	0·835	0·810	0·786	0·763	0·74	0·72
0·6	0·956	0·918	0·882	0·847	0·814	0·79	0·752			0·673
0·7	0·953	0·906	0·859	0·81						
0·8	0·941	0·86			0·667					0·480
0·9	0·875				0·471					
0·95	0·723				0·304					0·187
0·98	0·464									

$$-\frac{\pi v_x}{4U\vartheta}$$

ψ	$\varepsilon = 1{\cdot}1$	$\varepsilon = 1{\cdot}2$	$\varepsilon = 1{\cdot}3$	$\varepsilon = 1{\cdot}4$	$\varepsilon = 1{\cdot}5$
0	0·750	0·738	0·726	0·714	0·703
0·1	0·750	0·737	0·725	0·714	0·703
0·2	0·749	0·736	0·723	0·711	0·700
0·3	0·743	0·729	0·716	0·703	0·691
0·4	0·729	0·714	0·699	0·685	0·67
0·5					0·631
0·6					0·572
0·8					0·379
0·95					0·139

TABLE 2

Supervelocities along the Mid-chord Lines of Rhombus Wings for Different Values of Coefficient of Convergence ε. Bivonvex Parabolic Profile

Illustrated in Fig. 6

	$-\frac{\pi v_x}{4U\vartheta}$									
η'	$\varepsilon = 0{\cdot}1$	$\varepsilon = 0{\cdot}2$	$\varepsilon = 0{\cdot}3$	$\varepsilon = 0{\cdot}4$	$\varepsilon = 0{\cdot}5$	$\varepsilon = 0{\cdot}6$	$\varepsilon = 0{\cdot}7$	$\varepsilon = 0{\cdot}8$	$\varepsilon = 0{\cdot}9$	$\varepsilon = 1{\cdot}0$
0	0·958	0·925	0·897	0·872	0·850	0·829	0·811	0·794	0·779	0·764
0·1	0·982	0·949	0·919	0·892	0·868	0·847	0·827	0·809	0·793	0·777
0·2	0·993	0·972	0·947	0·924	0·897	0·875	0·855	0·836	0·818	0·802
0·3	0·998	0·987	0·969	0·948	0·927	0·905	0·885	0·867	0·849	0·832
0·4	1·001	0·997	0·986	0·970	0·953	0·935	0·917	0·899	0·881	0·865
0·5	1·003	1·004	1·000	0·991	0·978	0·964	0·948	0·933	0·917	0·902
0·6	1·005	1·009	1·011	1·008	1·001	0·991	0·979	0·965	0·951	0·937
0·7	1·006	1·014	1·021	1·025	1·023	1·019	1·012	1·002	0·991	0·979
0·8	1·008	1·019	1·032	1·042	1·048	1·050	1·049	1·044	1·039	1·031
0·9	1·009	1·026	1·046	1·065	1·080	1·092	1·101	1·106	1·107	1·107
0·95	—	1·031	1·057	1·084	1·108	1·129	1·146	1·159	1·168	1·174
0·99	1·014	1·116	1·153	1·193	1·232	1·269	1·297	1·331	1·355	1·374

TABLE 3

Velocity Distribution over a Rhombus Wing with Coefficient of Convergence $\varepsilon = 0{\cdot}3$. Biconvex Parabolic Profile

Illustrated in Figs. 8 and 13

	$-\frac{\pi v_x}{4U\vartheta}$					
ξ	$\eta' = 0$	$\eta' = 0{\cdot}1$	$\eta' = 0{\cdot}2$	$\eta' = 0{\cdot}5$	$\eta' = 0{\cdot}6$	$\eta' = 0{\cdot}7$
0	0·897	0·920	0·947	0·999	1·010	1·020
0·2	0·851	0·873	0·907	0·958	0·970	0·980
0·4	0·706	0·740	0·779	0·831	0·842	0·852
0·6	0·434	0·490	0·539	0·588	0·599	0·609
0·8	−0·057	0·039	0·115	0·137	0·147	0·157

TABLE 4

Supervelocities along the Mid-chord Lines of Cropped-Rhombus Wings with Taper Ratio $\psi = 0{\cdot}3$ and Different Values of Coefficient of Convergence ε. Biconvex Parabolic Profile

Illustrated in Fig. 10

	$-\frac{\pi v_x}{4U\vartheta}$					
η'	$\varepsilon = 0{\cdot}1$	$\varepsilon = 0{\cdot}2$	$\varepsilon = 0{\cdot}3$	$\varepsilon = 0{\cdot}5$	$\varepsilon = 0{\cdot}7$	$\varepsilon = 1{\cdot}0$
0	0·958	0·925	0·896	0·848	0·808	0·758
0·1	0·982	0·949	0·918	0·866	0·823	0·770
0·2	0·993	0·972	0·946	0·895	0·850	0·793
0·3	0·997	0·986	0·967	0·922	0·878	0·818
0·4	1·001	0·998	0·983	0·946	0·903	0·842
0·5	1·002	1·000	0·992	0·959	0·918	0·855
0·6	0·999	0·992	0·986	0·939	0·893	0·826
0·7	0·526	0·552	0·571	0·598	0·606	0·596

TABLE 5

Supervelocities along the Mid-chord Lines of Cropped-Rhombus Wings with Taper Ratio $\psi = 0{\cdot}6$ and Different Values of Coefficient of Convergence ε. Biconvex Parabolic Profile

Illustrated in Fig. 11

	$-\frac{\pi v_x}{4U\vartheta}$					
η'	$\varepsilon = 0{\cdot}1$	$\varepsilon = 0{\cdot}2$	$\varepsilon = 0{\cdot}3$	$\varepsilon = 0{\cdot}5$	$\varepsilon = 0{\cdot}7$	$\varepsilon = 1{\cdot}0$
0	0·956	0·918	0·882	0·814	0·752	0·673
0·1	0·979	0·934	0·900	0·826	0·759	0·676
0·2	0·988	0·948	0·912	0·828	0·756	0·669
0·3	0·977	0·923	0·875	0·783	0·710	0·628
0·4	0·522	0·535	0·536	0·525	0·504	0·470

It will be seen that in Tables 4 and 5 values of the supervelocity ratio have not been calculated for $\varepsilon = 0{\cdot}4$, $0{\cdot}6$, $0{\cdot}8$ and $0{\cdot}9$. The curves corresponding to these values shown in Figs. 10 and 11 were found by interpolation from the calculated values.

TABLE 6

Velocity Distribution over a Cropped-Rhombus Wing with Coefficient of Convergence $\varepsilon = 0{\cdot}3$ *and Taper Ratio* $\psi = 0{\cdot}3$. *Biconvex Parabolic Profile*

Illustrated in Figs. 9 and 14

	$-\frac{\pi v_x}{4U\vartheta}$		
ξ	$\eta' = 0{\cdot}5$	$\eta' = 0{\cdot}6$	$\eta' = 0{\cdot}7$
0	0·992	0·985	0·571
0·2	0·951	0·947	0·553
0·4	0·824	0·826	0·496
0·6	0·582	0·591	0·388
0·8	0·131	0·153	0·183

Only the outboard values of η' were taken for the velocity distribution over the cropped-rhombus wing with the parameters ε and ψ both equal to $0{\cdot}3$. This was because, for the inboard values of η', the supervelocities were nearly the same as for the full-rhombus wing and so these values (given by columns 2, 3 and 4 of Table 3) have been taken to be the same in both cases. It will be seen that even the values of supervelocities at $\eta' = 0{\cdot}5$ vary very little for the full-rhombus and the cropped wing with $\psi = 0{\cdot}3$ (*see* column 5 in Table 3 and column 2 in Table 6).

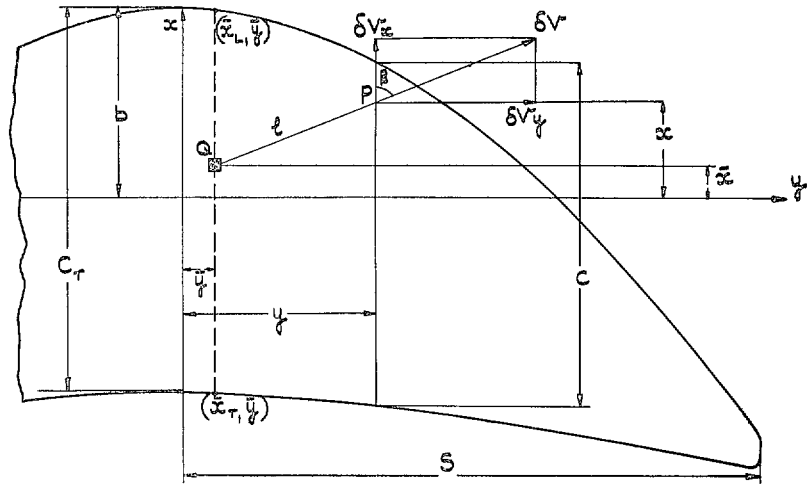

FIG. 1. Arbitrary wing plan form.

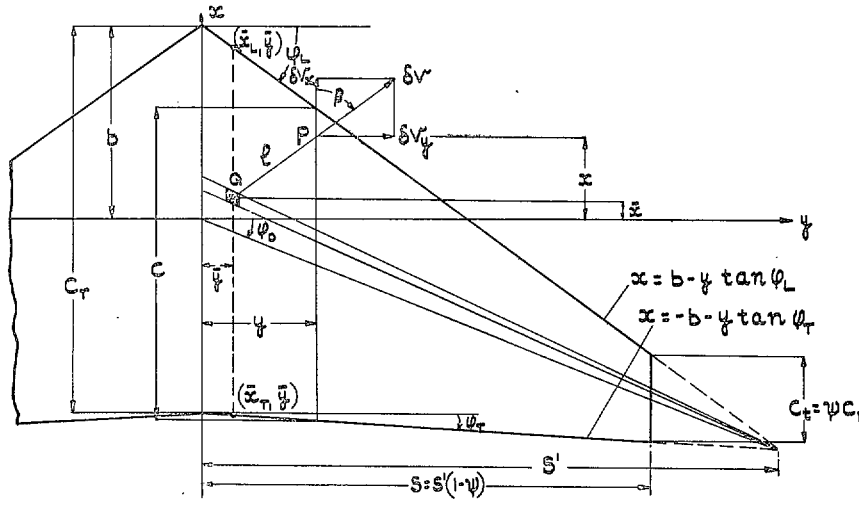

FIG. 2. Swept-back tapered wing plan form (full or cropped arrowhead).

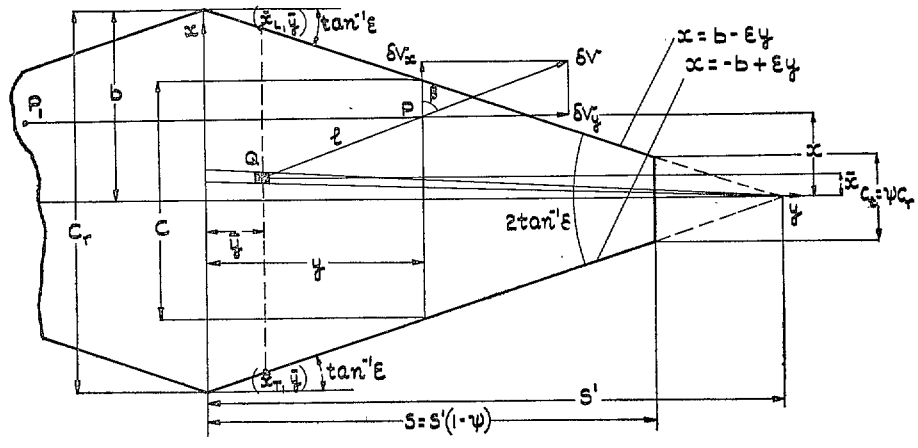

FIG. 3. Straight tapered wing plan form ($\varphi_0 = 0$, full or cropped rhombus).

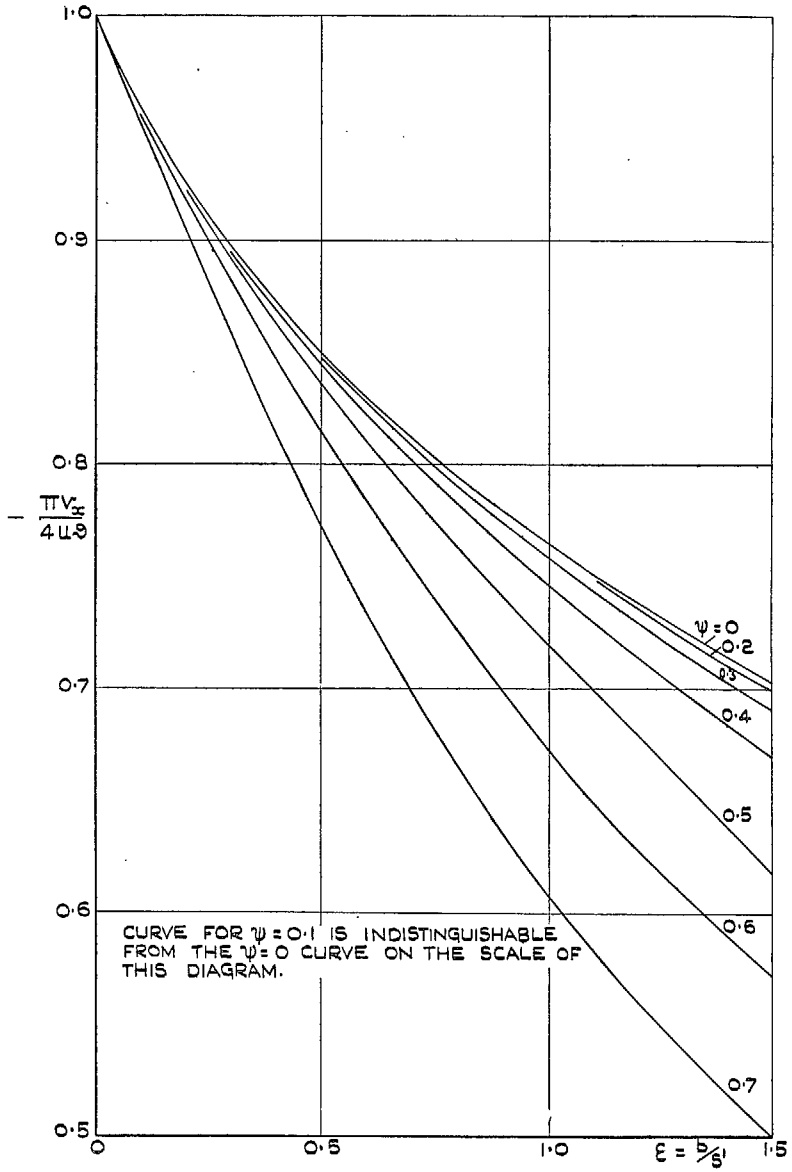

FIG. 4. Variation of supervelocities at the centres of straight tapered wings with coefficient of convergence ε, for different values of taper ratio ψ. Biconvex parabolic profile. From Table 1.

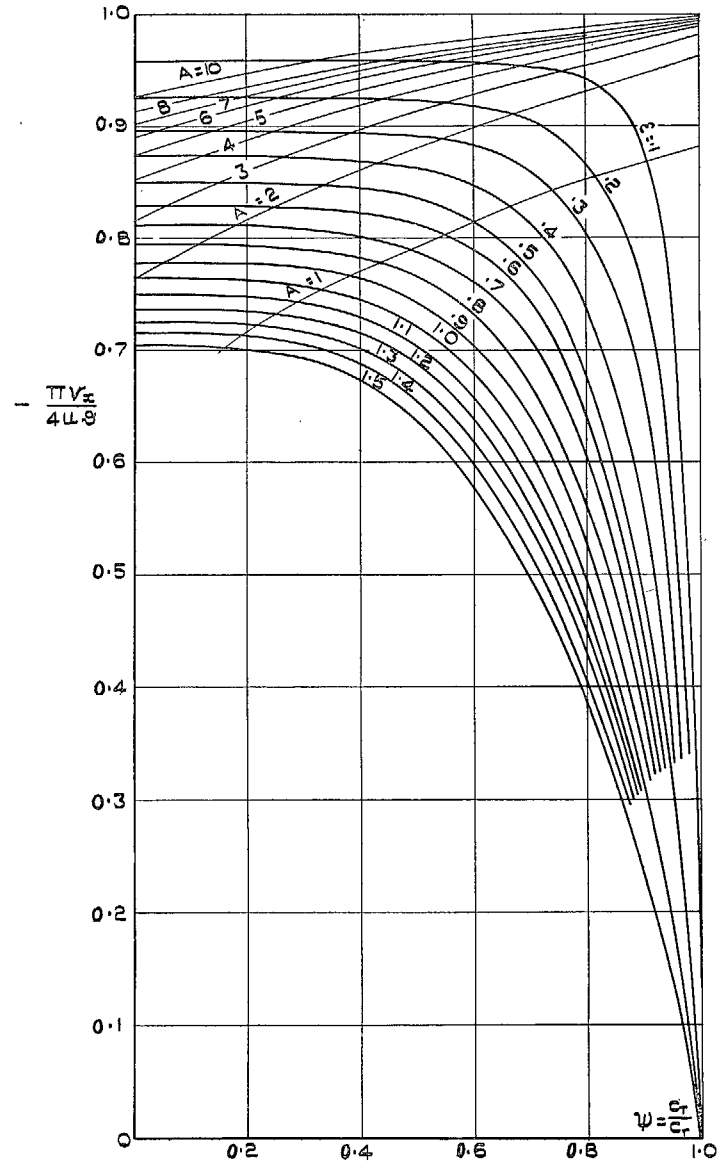

FIG. 5. Variation of supervelocities at the centres of straight tapered wings with taper ratio ψ for different values of coefficient of convergence ε. Biconvex parabolic profile. Curves of constant aspect ratio A shown as thin lines. From Table 1.

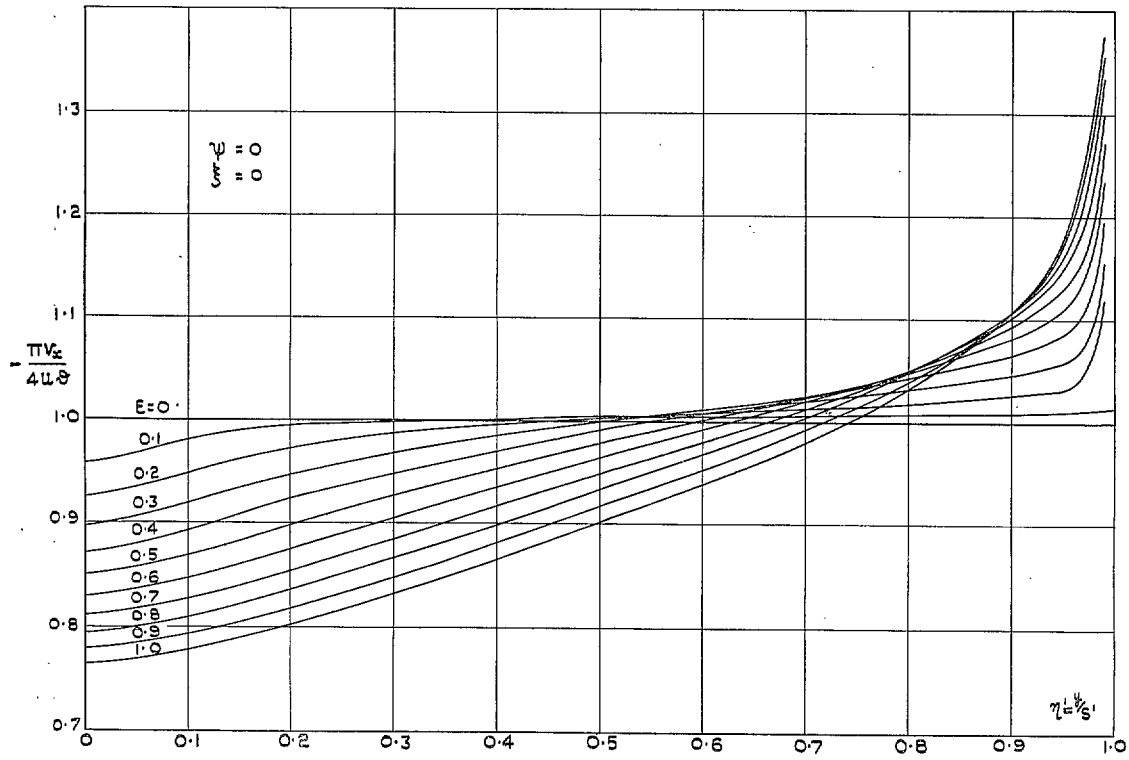

FIG. 6. Supervelocities along mid-chord lines of rhombus wings for different values of coefficient of convergence ε. Biconvex parabolic profile. From Table 2.

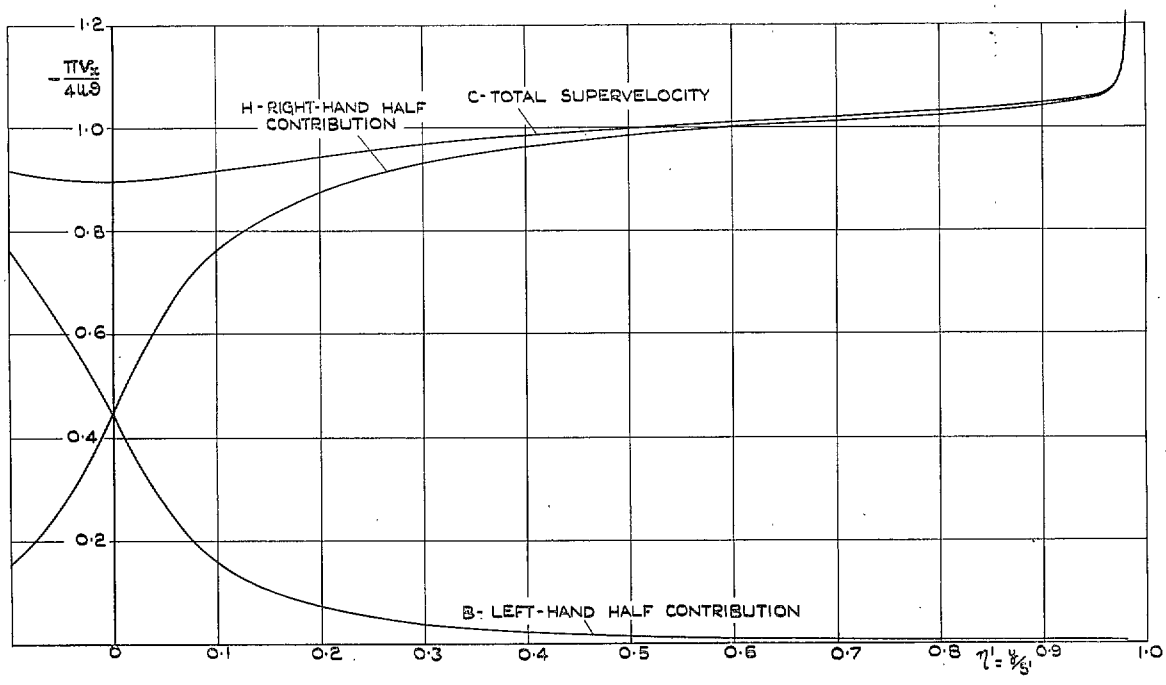

FIG. 7. Contributions of the two half-wings to the supervelocities along the mid-chord line of the right half of a rhombus wing, with $\varepsilon = 0{\cdot}3$.

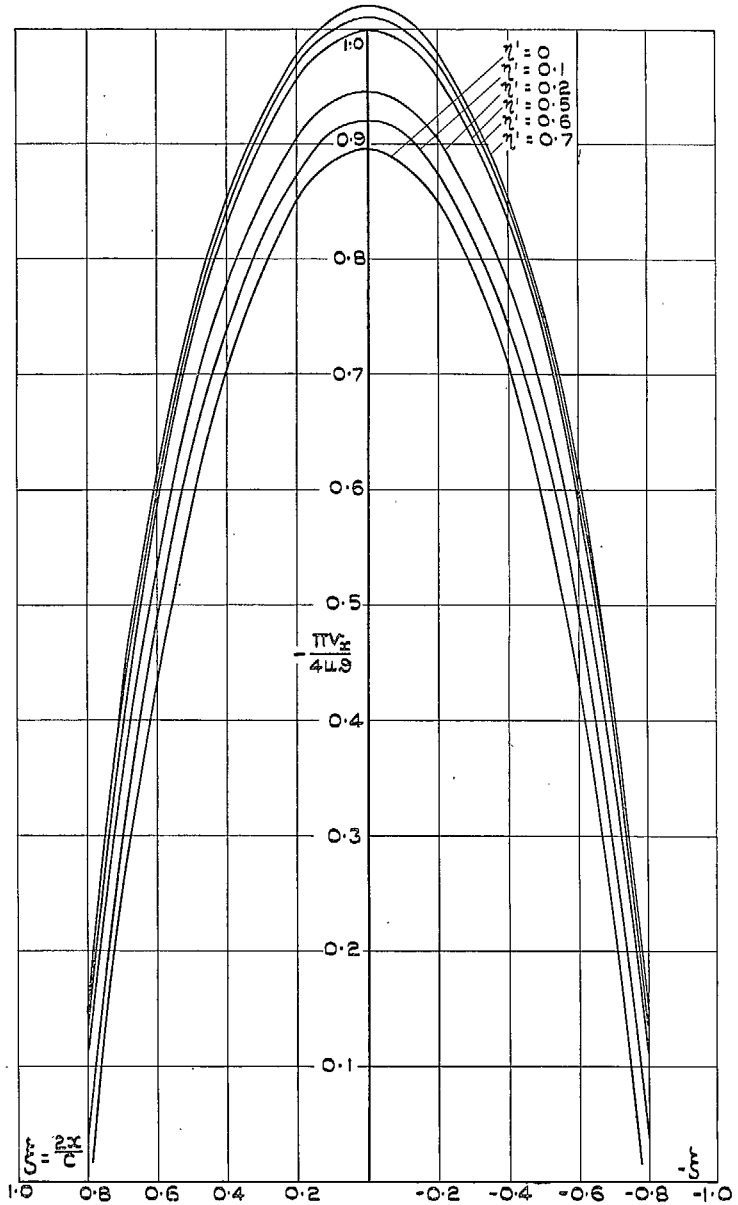

FIG. 8. Velocity distribution over rhombus wing with coefficient of convergence $\varepsilon = 0{\cdot}3$. Biconvex parabolic profile. From Table 3.

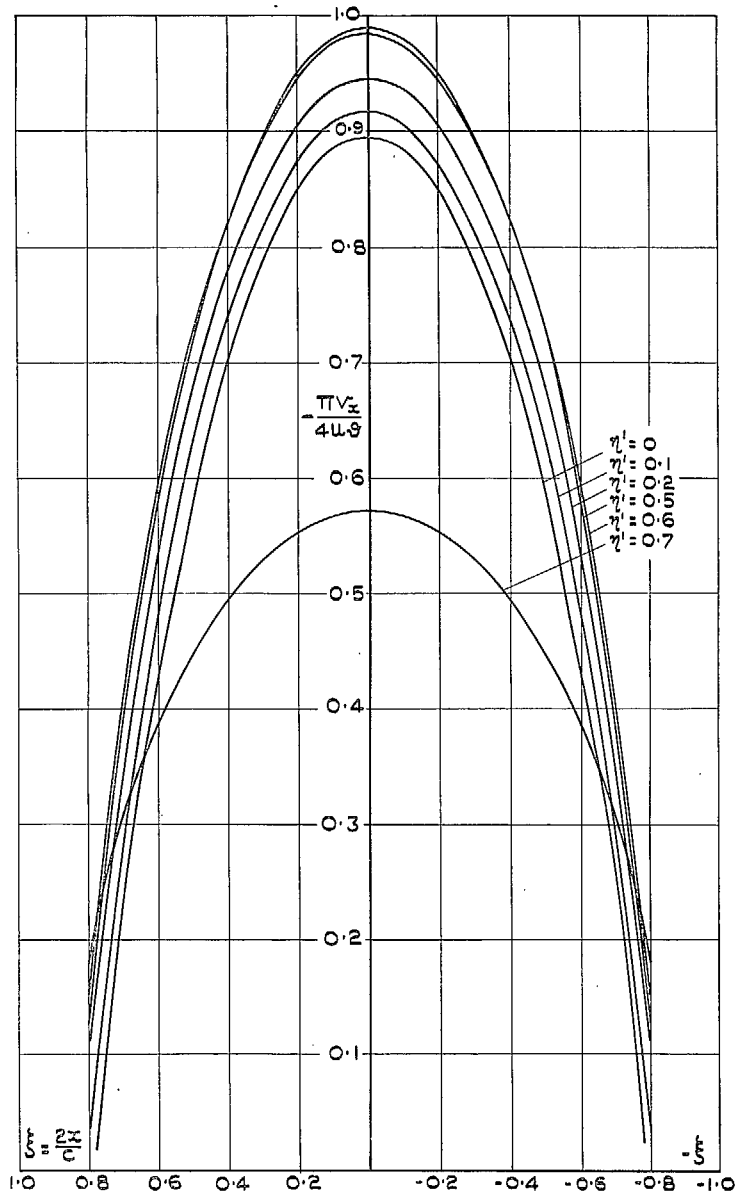

FIG. 9. Velocity distribution over cropped-rhombus wing with coefficient of convergence $\varepsilon = 0{\cdot}3$, and taper ratio $\psi = 0{\cdot}3$. Biconvex parabolic profile. From Table 6.

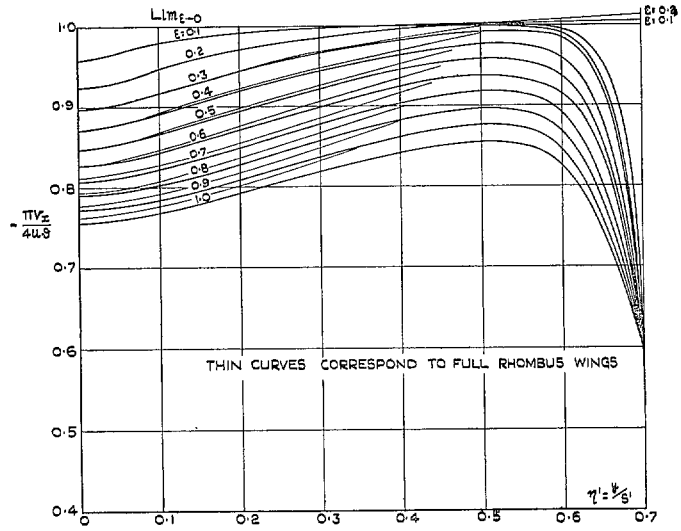

FIG. 10. Supervelocities along mid-chord lines of cropped-rhombus wings with taper ratio $\psi = 0{\cdot}3$, for different values of coefficient of convergence ε. Biconvex parabolic profile. From Table 4.

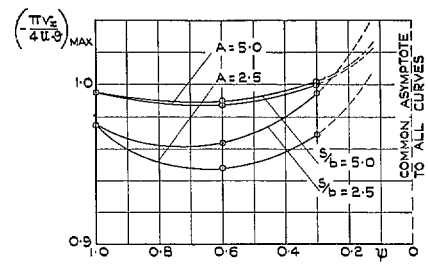

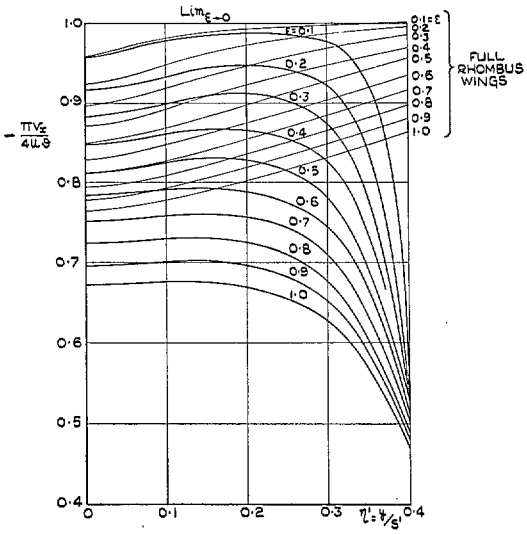

FIG. 11. Supervelocities along mid-chord lines of cropped-rhombus wings with taper ratio $\psi = 0{\cdot}6$, for different values of coefficient of convergence ε. Biconvex parabolic profile. From Table 5.

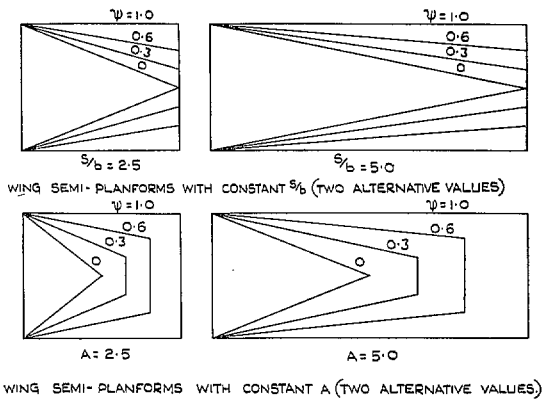

FIG. 12. Variation of maximum supervelocity with taper ratio ψ for unswept wings with constant s/b or constant aspect ratio A.

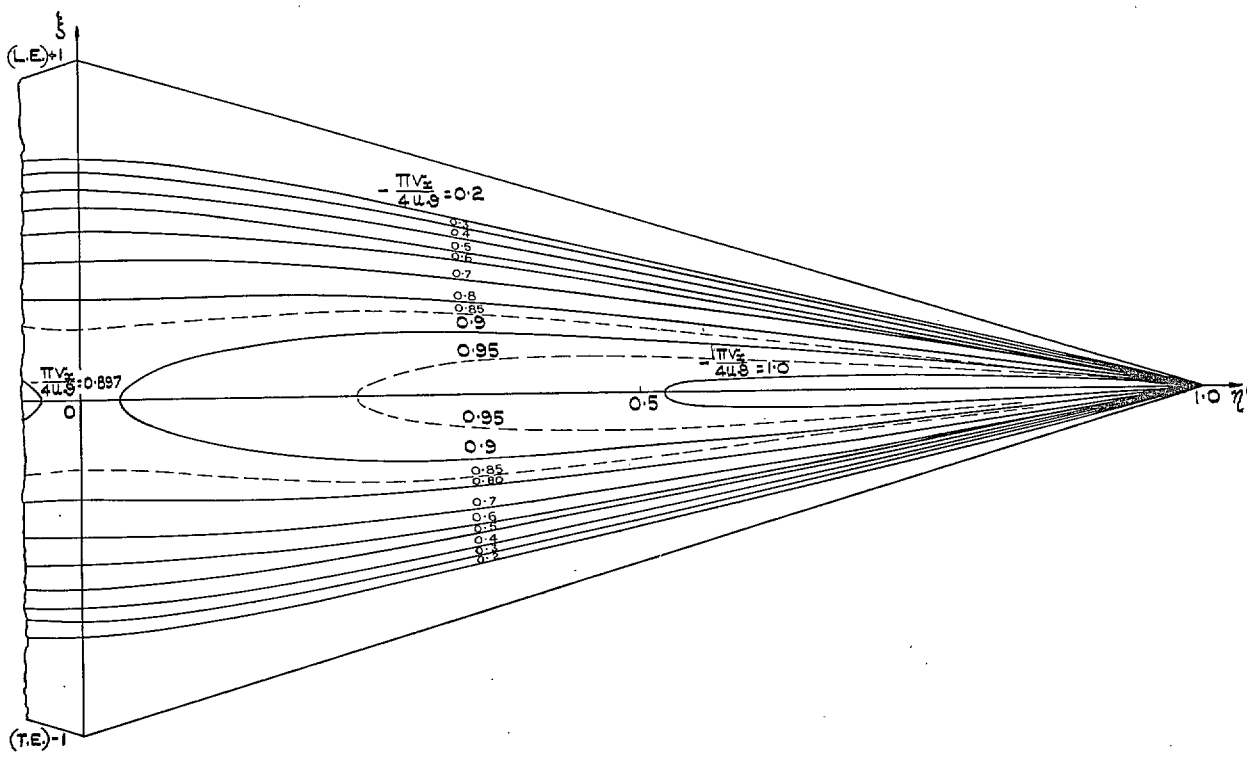

FIG. 13. Isobars over rhombus wing with coefficient of convergence $\varepsilon = 0 \cdot 3$. Biconvex parabolic profile. From Table 3.

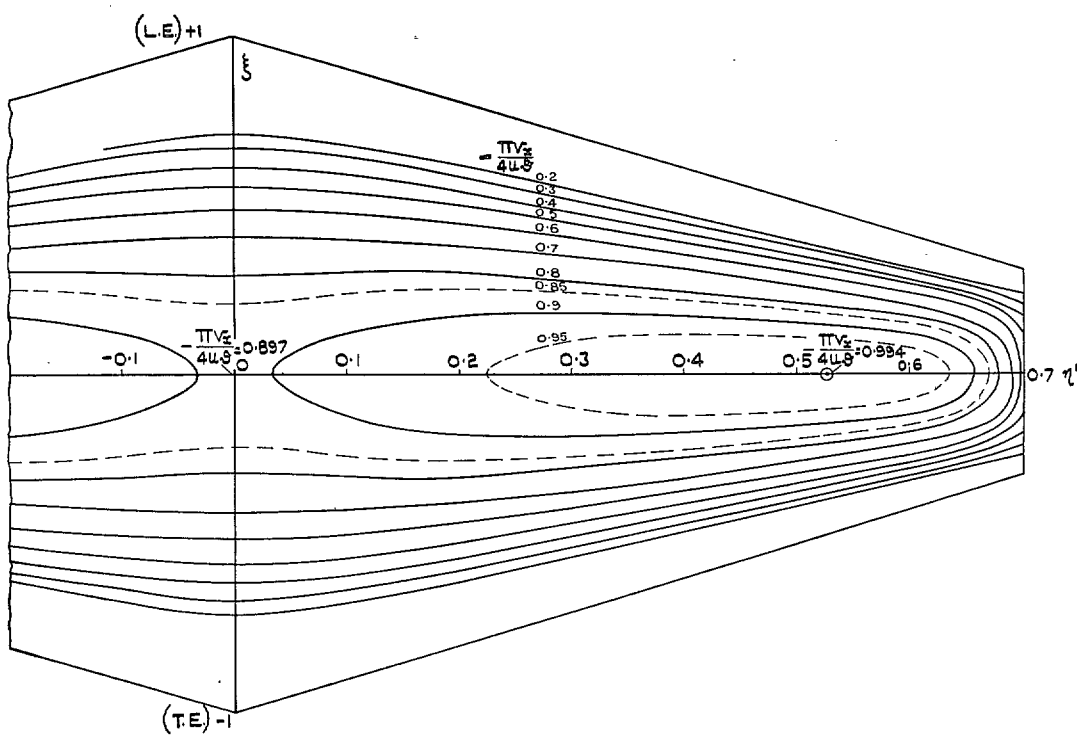

FIG. 14. Isobars over cropped-rhombus wing with coefficient of convergence $\varepsilon = 0 \cdot 3$ and taper ratio $\psi = 0 \cdot 3$. Biconvex parabolic profile. From Table 6.

(57975) Wt. 17/680 K.9 6/54 Hw.

PRINTED IN GREAT BRITAIN

Publications of the Aeronautical Research Council

ANNUAL TECHNICAL REPORTS OF THE AERONAUTICAL RESEARCH COUNCIL (BOUND VOLUMES)

1936 Vol. I. Aerodynamics General, Performance, Airscrews, Flutter and Spinning. 40*s.* (40*s.* 9*d.*)
Vol. II. Stability and Control, Structures, Seaplanes, Engines, etc. 50*s.* (50*s.* 10*d.*)

1937 Vol. I. Aerodynamics General, Performance, Airscrews, Flutter and Spinning. 40*s.* (40*s.* 10*d.*)
Vol. II. Stability and Control, Structures, Seaplanes, Engines, etc. 60*s.* (61*s.*)

1938 Vol. I. Aerodynamics General, Performance, Airscrews. 50*s.* (51*s.*)
Vol. II. Stability and Control, Flutter, Structures, Seaplanes, Wind Tunnels, Materials. 30*s.* (30*s.* 9*d.*)

1939 Vol. I. Aerodynamics General, Performance, Airscrews, Engines. 50*s.* (50*s.* 11*d.*)
Vol. II. Stability and Control, Flutter and Vibration, Instruments, Structures, Seaplanes, etc. 63*s.* (64*s.* 2*d.*)

1940 Aero and Hydrodynamics, Aerofoils, Airscrews, Engines, Flutter, Icing, Stability and Control, Structures, and a miscellaneous section. 50*s.* (51*s.*)

1941 Aero and Hydrodynamics, Aerofoils, Airscrews, Engines, Flutter, Stability and Control, Structures. 63*s.* (64*s.* 2*d.*)

1942 Vol. I. Aero and Hydrodynamics, Aerofoils, Airscrews, Engines. 75*s.* (76*s.* 3*d.*)
Vol. II. Noise, Parachutes, Stability and Control, Structures, Vibration, Wind Tunnels. 47*s.* 6*d.* (48*s.* 5*d.*)

1943 Vol. I. (*In the press.*)
Vol. II. (*In the press.*)

ANNUAL REPORTS OF THE AERONAUTICAL RESEARCH COUNCIL—

1933–34	1*s.* 6*d.* (1*s.* 8*d.*)	1937	2*s.* (2*s.* 2*d.*)
1934–35	1*s.* 6*d.* (1*s.* 8*d.*)	1938	1*s.* 6*d.* (1*s.* 8*d.*)
April 1, 1935 to Dec. 31, 1936.	4*s.* (4*s.* 4*d.*)	1939–48	3*s.* (3*s.* 2*d.*)

INDEX TO ALL REPORTS AND MEMORANDA PUBLISHED IN THE ANNUAL TECHNICAL REPORTS, AND SEPARATELY—

April, 1950 - - - - R. & M. No. 2600. 2*s.* 6*d.* (2*s.* 7½*d.*)

AUTHOR INDEX TO ALL REPORTS AND MEMORANDA OF THE AERONAUTICAL RESEARCH COUNCIL—

1909–1949. R. & M. No. 2570. 15*s.* (15*s.* 3*d.*)

INDEXES TO THE TECHNICAL REPORTS OF THE AERONAUTICAL RESEARCH COUNCIL—

December 1, 1936 — June 30, 1939.	R. & M. No 1850.	1*s.* 3*d.* (1*s.* 4½*d.*)
July 1, 1939 — June 30, 1945.	R. & M. No. 1950.	1*s.* (1*s.* 1½*d.*)
July 1, 1945 — June 30, 1946.	R. & M. No. 2050.	1*s.* (1*s.* 1½*d.*)
July 1, 1946 — December 31, 1946.	R. & M. No. 2150.	1*s.* 3*d.* (1*s.* 4½*d.*)
January 1, 1947 — June 30, 1947.	R. & M. No. 2250.	1*s.* 3*d.* (1*s.* 4½*d.*)
July, 1951.	R. & M. No. 2350.	1*s.* 9*d.* (1*s.* 10½*d.*)

Prices in brackets include postage.

Obtainable from

HER MAJESTY'S STATIONERY OFFICE

York House, Kingsway, London, W.C.2; 423 Oxford Street, London, W.1 (Post Orders: P.O. Box 569, London, S.E.1); 13a Castle Street, Edinburgh 2; 39, King Street, Manchester, 2; 2 Edmund Street, Birmingham 3; 1 St. Andrew's Crescent, Cardiff; Tower Lane, Bristol 1; 80 Chichester Street, Belfast, or through any bookseller

S.O. Code No. 23-2858